ARTICLES
https://doi.org/10.1038/s41587-022-01381-4

nature biotechnology

Generation of a live attenuated influenza A vaccine by proteolysis targeting

Longlong Si[1,17] ✉, Quan Shen[1,17], Jing Li[1,17], Li Chen[1], Jinying Shen[1], Xue Xiao[1], Haiqing Bai[2], Tang Feng[3], Adam Yongxin Ye[4], Le Li[1], Chunhe Zhang[1,3], Zhen Li[1], Ping Wang[1], Crystal Yuri Oh[5], Atiq Nurani[6], Siwen Niu[7], Chengxin Zhang[8], Xiaoqiong Wei[8], Wanqiong Yuan[9,10,11], Hao Liao[12], Xiaojie Huang[13], Ning Wang[13], Wen-xia Tian[14], Hongwei Tian[15], Li Li[4], Xiaoheng Liu[3] and Roberto Plebani[16]

The usefulness of live attenuated virus vaccines has been limited by suboptimal immunogenicity, safety concerns or cumbersome manufacturing processes and techniques. Here we describe the generation of a live attenuated influenza A virus vaccine using proteolysis-targeting chimeric (PROTAC) technology to degrade viral proteins via the endogenous ubiquitin–proteasome system of host cells. We engineered the genome of influenza A viruses in stable cell lines engineered for virus production to introduce a conditionally removable proteasome-targeting domain, generating fully infective PROTAC viruses that were live attenuated by the host protein degradation machinery upon infection. In mouse and ferret models, PROTAC viruses were highly attenuated and able to elicit robust and broad humoral, mucosal and cellular immunity against homologous and heterologous virus challenges. PROTAC-mediated attenuation of viruses may be broadly applicable for generating live attenuated vaccines.

Live attenuated virus vaccines have been generated by several strategies, including cold-adapted live attenuated influenza vaccines (CAIVs), codon-deoptimized virus, premature termination codon-harboring virus, hyper-interferon-sensitive virus and viral-protein-altered virus[1–12]. However, current attenuation strategies are often accompanied by decrease or loss of safety, efficacy or productivity[1,13–16]. In addition, immune escape due to rapid viral evolution poses a further challenge for traditional influenza vaccines[1,13]. Thus, there is an urgent need for new vaccine approaches that could enable the generation of safer and more effective live vaccines in a simpler way[2].

Results

Generation and characterization of PROTAC influenza virus. Given that virus replication depends on virally encoded proteins[17], manipulation of viral protein stability by using the protein degradation machinery of the host cell[18–23] may represent a potential approach to switch the viral life cycle on and off for vaccine development (Fig. 1a). To this aim, PROTAC viruses were designed by fusing a conditionally removable proteasome-targeting domain (PTD) to influenza viral proteins (Fig. 1a,b). The PTD was designed to contain a proteasome-targeting peptide, ALAPYIP, and a tobacco etch virus cleavage site (TEVcs) linker, ENLYFQG (Fig. 1b). It has been well-characterized that ALAPYIP is recognized by the von Hippel–Lindau tumor suppressor protein (VHL), the substrate recognition component of $CRL2^{VHL}$ E3 ubiquitin ligase, leading to polyubiquitination and, thus, degradation of tagged proteins by proteasome[24–27]. The ubiquitous expression of VHL in most normal tissues and cell types could provide a critical basis with respect to the safety of PROTAC vaccines (Extended Data Figs. 1 and 2)[28–31]. In addition, an in silico homology/identify search of PTD sequence in the human proteome from the UniProt Knowledge Base and in the known peptide major histocompatibility complex (MHC) sequence library from the Immune Epitope Database (http://www.iedb.org/) revealed the lack of peptide with high sequence homology to PTD, eliminating the potential risk of PTD to evoke an autoimmune response. Therefore, the PTD was used to selectively induce proteasomal degradation of viral proteins of interest; however, the TEVcs linker could be selectively cleaved by the tobacco etch virus protease (TEVp) to separate the viral proteins from the PTD, sparing them from degradation.

To achieve this design, we first generated TEVp-expressing stable cell lines to maintain the reproductive potential of PROTAC viruses during vaccine production. Human embryonic kidney (HEK) 293T cells and Madin–Darby canine kidney (MDCK.2) cells were transduced with lentivector for stable integration of the

[1]CAS Key Laboratory of Quantitative Engineering Biology, Shenzhen Institute of Synthetic Biology, Shenzhen Institute of Advanced Technology, Chinese Academy of Sciences, Shenzhen, China. [2]Wyss Institute for Biologically Inspired Engineering at Harvard University, Boston, MA, USA. [3]Institute of Biomedical Engineering, West China School of Basic Medical Sciences & Forensic Medicine, Sichuan University, Chengdu, China. [4]Department of Genetics, Harvard Medical School, Boston, MA, USA. [5]Rare Disease Research Unit, Pfizer Inc., Cambridge MA, USA. [6]Jnana Therapeutics, Boston, MA, USA. [7]Third Institute of Oceanography, State Oceanic Administration, Xiamen, China. [8]Department of Computational Medicine and Bioinformatics, University of Michigan, Ann Arbor, MI, USA. [9]Department of Orthopedics, Peking University Third Hospital, Beijing, China. [10]Beijing Key Laboratory of Spinal Disease, Beijing, China. [11]Engineering Research Center of Bone and Joint Precision Medicine, Beijing, China. [12]Department of Clinical Laboratory, Shenzhen Third People's Hospital, Southern University of Science and Technology, National Clinical Research Center for Infectious Diseases, Shenzhen, China. [13]Shenzhen Institute of Advanced Technology, Chinese Academy of Sciences, Shenzhen, China. [14]College of Veterinary Medicine, Shanxi Agricultural University, Jinzhong, China. [15]National and Local Joint Engineering Research Center of Biodiagnosis and Biotherapy, The Second Affiliated Hospital of Xi'an Jiaotong University, Xi'an, China. [16]Center on Advanced Studies and Technology (CAST), Department of Medical, Oral and Biotechnological Sciences, 'G. d'Annunzio' University of Chieti-Pescara, Chieti, Italy. [17]These authors contributed equally: Longlong Si, Quan Shen, Jing Li. ✉e-mail: ll.si@siat.ac.cn

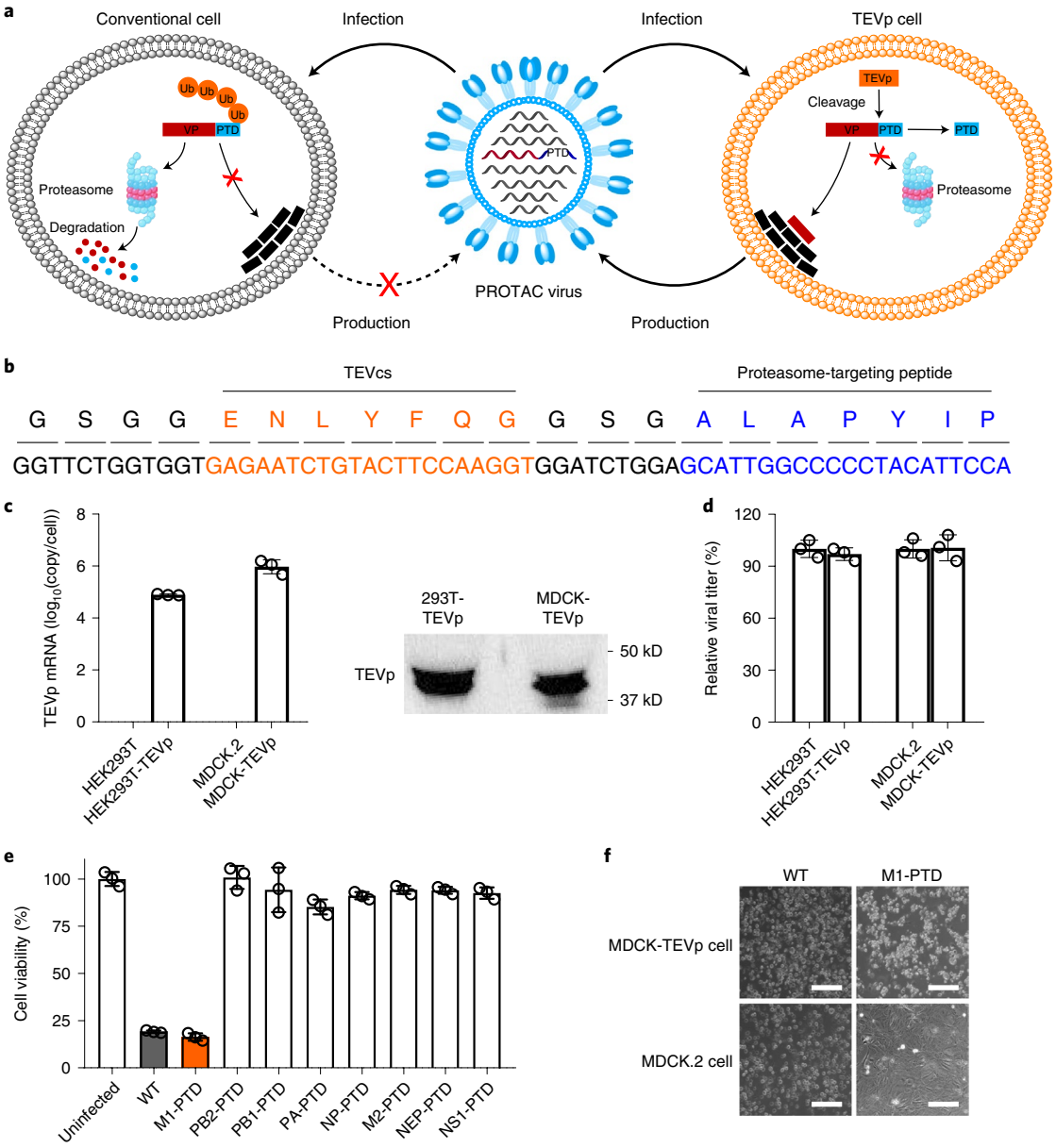

Fig. 1 | Establishment of the PROTAC virus production system. a, Schematic illustration of the generation of PROTAC viruses that are highly reproductive in TEVp-expressing stable cells but live attenuated by proteasome-mediated viral protein destabilization in conventional cells. VP, viral protein; Ub, ubiquitin. **b**, Sequences of amino acids and gene of PTD. The proteasome-targeting peptide is depicted in blue, and the TEVcs is depicted in orange. **c**, Characterization of engineered PROTAC virus-producing stable cell lines by the expression of TEVp measured by qPCR and western blotting. Data are presented as mean ± s.d.; $n = 3$ biological replicates. **d**, Comparison of the capabilities of TEVp-expressing stable cell lines and their parental cell lines to propagate WT influenza viruses. Data are presented as mean ± s.d.; $n = 3$ biological replicates. **e**, Characterization of the generation of PROTAC viruses by the CPE by inoculating putative viruses in MDCK-TEVp cells. CPE was measured 4–5 days after inoculation by CellTiter-Glo assay. Data are presented as mean ± s.d.; $n = 3$ biological replicates. **f**, Characterization of TEVp-dependent replication of M1-PTD by CPE. Cells were infected with M1-PTD or WT virus (MOI = 0.01), and CPE was observed 4 days after infection ($n = 3$). Scale bar, 200 μm.

TEVp gene into the host genome. The resultant stable cell lines, HEK293T-TEVp and MDCK-TEVp, were selected and verified by the TEVp expression measured by quantitative polymerase chain reaction (qPCR) and western blotting (Fig. 1c). The capabilities of the stable cell lines to propagate wild-type (WT) viruses were tested in parallel with the respective parental cell lines by inoculation with influenza A/WSN/33 (H1N1) virus. Plaque formation assay indicated equal viral propagation efficiencies between each stable cell line and its corresponding parental cell line (Fig. 1d).

We next selected eight viral proteins (M1, PB2, PB1, PA, NP, M2, NEP and NS1) for the incorporation of PTD (Fig. 1b and Extended Data Fig. 3). The resultant PTD-containing viral genes were individually used to generate PROTAC viruses in co-cultured HEK293T-TEVp/MDCK-TEVp cells (Fig. 1a). The putative PROTAC viruses were amplified in MDCK-TEVp cells, and their production and infectivity were verified by the cytopathic effects (CPEs) caused by viral infection (Fig. 1e). M1-PTD caused obvious CPE in MDCK-TEVp cells, whereas no CPE was detected for

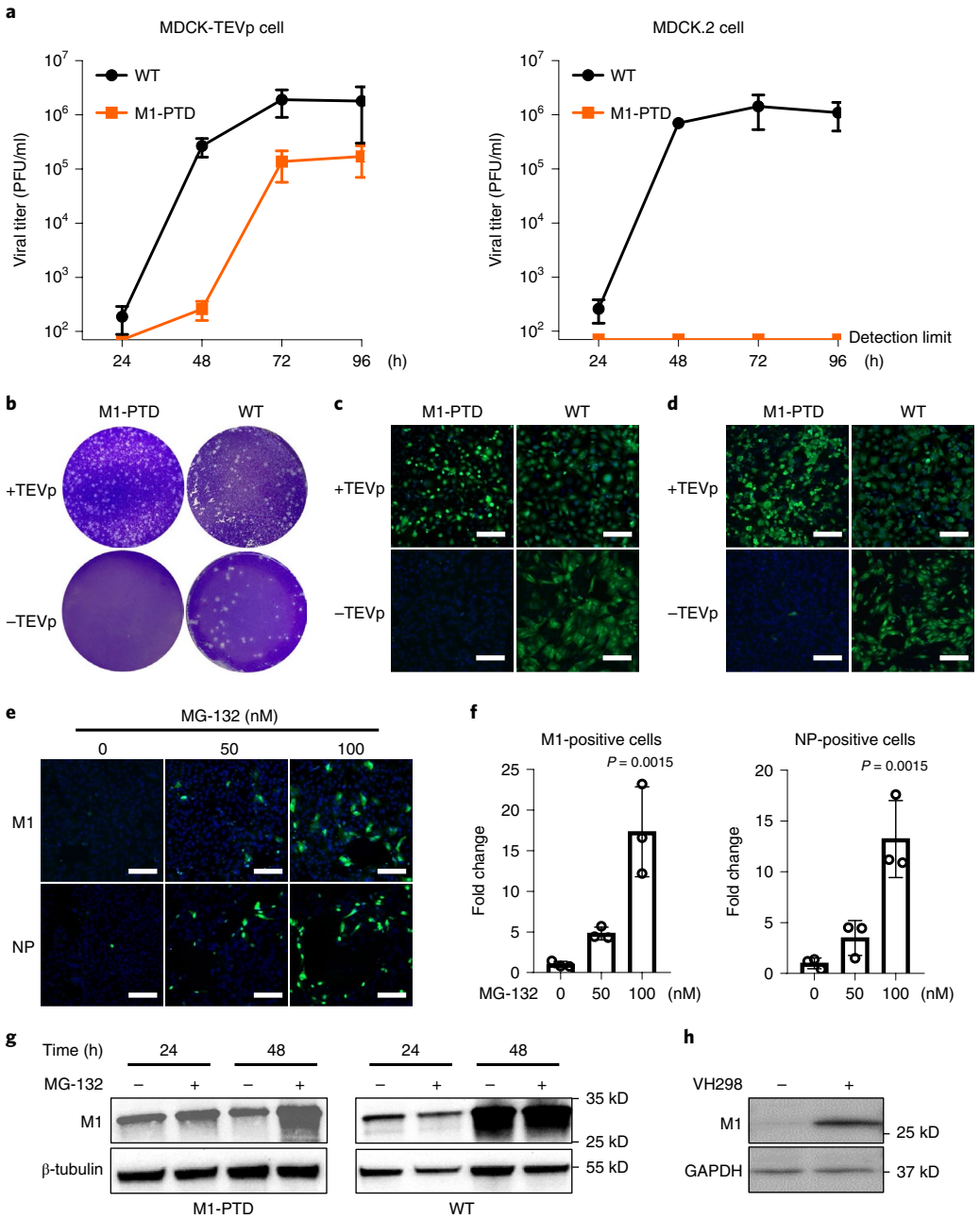

Fig. 2 | Characterization of PROTAC virus M1-PTD. a, Multicycle replication kinetic curves of M1-PTD in MDCK-TEVp and conventional MDCK.2 cells. Data are presented as mean ± s.d.; $n = 3$ biological replicates. The detection limit is 70 PFU/mL. **b**, Comparisons of the plaque phenotypes of M1-PTD and WT virus in MDCK-TEVp (+TEVp) and conventional MDCK.2 (−TEVp) cells. Obvious plaque formation, representing viral propagation in cells, was observed only in MDCK-TEVp cells and not in MDCK.2 cells for M1-PTD ($n = 3$). **c**, Immunofluorescence staining of influenza viral M1 at 48 hours after infection (MOI = 0.01) showing robust replication of M1-PTD only in MDCK-TEVp cells (+TEVp) and not in MDCK.2 cells (−TEVp). Representative images are shown for each condition ($n = 3$). Green, M1; blue, nuclei; scale bar, 100 μm. **d**, Immunofluorescence staining of influenza viral NP at 48 hours after infection (MOI = 0.01) showing robust replication of M1-PTD only in MDCK-TEVp cells (+TEVp) and not in MDCK.2 cells (−TEVp). Representative images are shown for each condition ($n = 3$). Green, NP; blue, nuclei; scale bar, 100 μm. **e**,**f**, Immunofluorescence staining of influenza viral M1 and NP staining at 48 hours after infection (MOI = 0.01) showing the replication competence of M1-PTD in conventional MDCK.2 cells in the absence and presence of MG-132 (**e**). Data represent the fold change of infected cells (M1-positive and NP-positive) by quantitatively analyzing three representative areas from each condition (**f**). Data are presented as mean ± s.d.; $n = 3$ biological replicates; one-way ANOVA with Dunnett's multiple comparisons test. Green, M1 or NP; blue, nuclei; scale bar, 100 μm. **g**, PTD-mediated viral M1 protein degradation is dependent on the proteasome. Conventional MDCK.2 cells were infected with M1-PTD or WT viruses (MOI = 0.1) in the absence and presence of proteasome inhibitor MG-132 (50 nM) and analyzed for viral M1 protein levels by western blotting at indicated times ($n = 3$). **h**, PTD-mediated viral M1 protein degradation is dependent on the VHL E3 ubiquitin ligase. Conventional MDCK.2 cells were infected with M1-PTD (MOI = 0.1) in the absence and presence of 200 μM VH298, an inhibitor of VHL E3 ubiquitin ligase, and analyzed for viral M1 protein levels by western blotting at 48 hours after infection ($n = 3$).

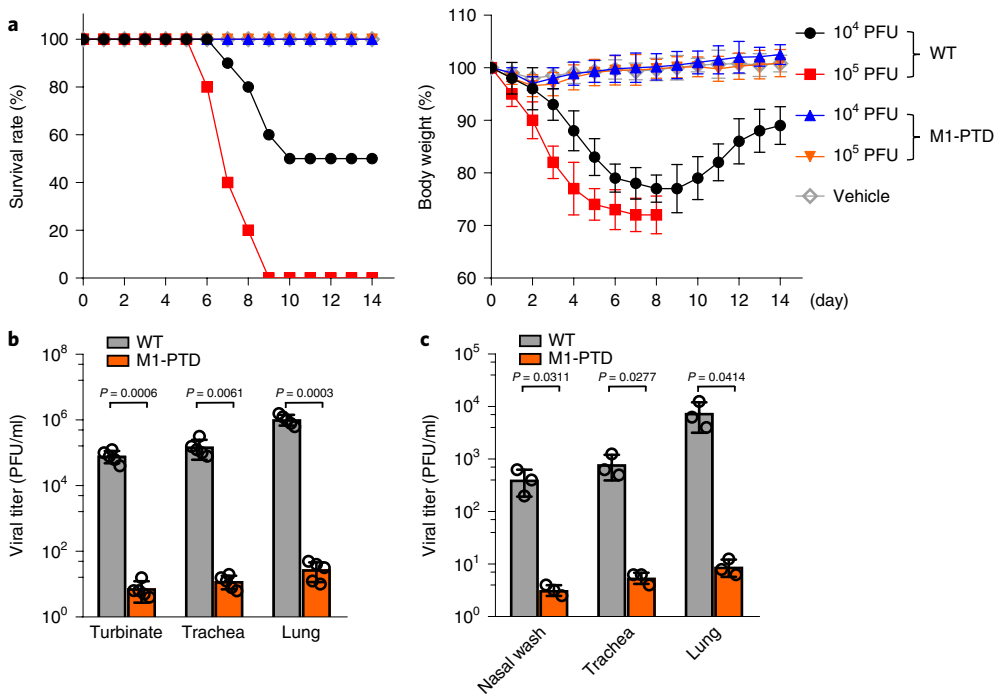

Fig. 3 | Evaluation of the in vivo safety of PROTAC virus M1-PTD in mice and ferrets. a, Survival rates and body weights of mice ($n = 10$) after intranasal infection with the indicated viruses. Data are presented as mean ± s.d. **b**, Viral titers in mouse tissues ($n = 5$) at day 3 after infection with 10^5 PFU of indicated viruses. Data are plotted for individual mice and overlaid with mean ± s.d.; unpaired two-tailed *t*-test. **c**, Viral titers in different organs of ferrets ($n = 3$) at day 3 after infection with 10^5 PFU of WT WSN or M1-PTD. Data are plotted for individual ferrets and overlaid with mean ± s.d.; unpaired two-tailed *t*-test.

PB2-PTD, PB1-PTD, PA-PTD, NP-PTD, M2-PTD, NEP-PTD or NS1-PTD (Fig. 1e). Quantification of viral titers by the median tissue culture infectious dose ($TCID_{50}$) assay and the plaque formation assay indicated that the viral titers of M1-PTD could reach to ~10^6 plaque-forming units per milliliter (PFU/ml) after expansion in MDCK-TEVp cells, similar to those of WT virus (10^6–2×10^6 PFU/mL), suggesting a high propagation efficiency of M1-PTD in MDCK-TEVp cells. Notably, the CPE caused by M1-PTD was observed only in MDCK-TEVp cells and not in the conventional MDCK.2 cells (Fig. 1f), indicating the successful generation of TEVp-dependent M1-PTD. The differences between M1-PTD and other PROTAC viral strains could be partially explained by the conformations of PTD within its tagged viral proteins: the TEVcs is buried inside the other viral proteins while the proteolysis-targeting peptide is exposed (Extended Data Fig. 4), leading to low cleavage efficiency of the TEVcs and high proteolysis efficiency, as shown by protein structure prediction[32].

The safety of PROTAC viruses as potential vaccines heavily depends on their degrees of attenuation in conventional cells. To quantify the attenuation of M1-PTD, we measured replication kinetics of M1-PTD and WT virus in MDCK-TEVp and MDCK.2 cells at a multiplicity of infection (MOI) of 0.01 (Fig. 2a). M1-PTD exhibited efficient replication only in MDCK-TEVp cells and not in MDCK.2 cells (Fig. 2a). The incorporation of PTD to M1 has minimal effect on endpoint titer of M1-PTD relative to WT virus in MDCK-TEVp cells (Fig. 2a), confirming the high production efficiency of M1-PTD in MDCK-TEVp cells. In contrast, viral titers of progeny M1-PTD expanded in MDCK.2 cells were below the limit of detection, indicating a significant decrease in the replication competence by a factor of $>2 \times 10^4$ relative to WT virus (Fig. 2a). These data suggest that the conditional destabilization of viral M1 is sufficient to reversibly suppress viral replication, which was verified by plaque formation assay (Fig. 2b) and immunofluorescence staining of viral M1 and NP proteins (Fig. 2c,d), respectively. These results suggest that PROTAC virus M1-PTD may be safer than a CAIV generated by the live attenuated vaccine approach used in FluMist, the replication competence of which was decreased by a factor of only ~100 relative to WT virus at 37 °C[6,33]. Notably, M1-PTD was genetically stable even over 20 passages (Extended Data Fig. 5).

We then confirmed that the PTD-mediated viral protein degradation and attenuation of PROTAC virus are proteasome dependent by amplifying M1-PTD1 virus in conventional MDCK.2 cells in the presence and absence of the proteasome inhibitor MG-132: the inhibition of proteasome by MG-132 restored the viral replication competence (Fig. 2e,f) and M1 protein levels (Fig. 2g) of M1-PTD in a dose-dependent manner. In addition, inhibition of VHL E3 ubiquitin ligase by VH298 reduced viral M1 protein degradation in M1-PTD virus-infected MDCK.2 cells (Fig. 2h), confirming the VHL E3 ubiquitin ligase dependence of the viral protein degradation of PROTAC virus. Finally, M1-PTD infection did not influence protein levels of HIF-1α, the endogenous substrate of VHL, even at the highest multiplicity of infection (MOI = 1) (Extended Data Fig. 6), eliminating the potential adverse effect due to substrate competition.

PROTAC virus is highly attenuated in mice and ferrets. We next evaluated the in vivo safety of M1-PTD by intranasally infecting BALB/c mice and ferrets, the commonly used animal models for influenza studies. The median lethal dose (LD_{50}) of WT virus in mice was 10^4 PFU, and $10 \times LD_{50}$ of WT virus caused the death of all mice, accompanied by obvious body weight loss (Fig. 3a). In contrast, no death, weight loss or other indicative clinical symptoms were observed in M1-PTD-infected mice at the same dosages (Fig. 3a). By day 3 after inoculation with 10^5 PFU of WT or M1-PTD viruses, titers of M1-PTD in mouse turbinate, trachea and lung were $10^{0.81}$, $10^{1.06}$ and $10^{1.38}$ PFU/mL, respectively, which were significantly lower than those of WT virus (~4-log, ~4.1-log and

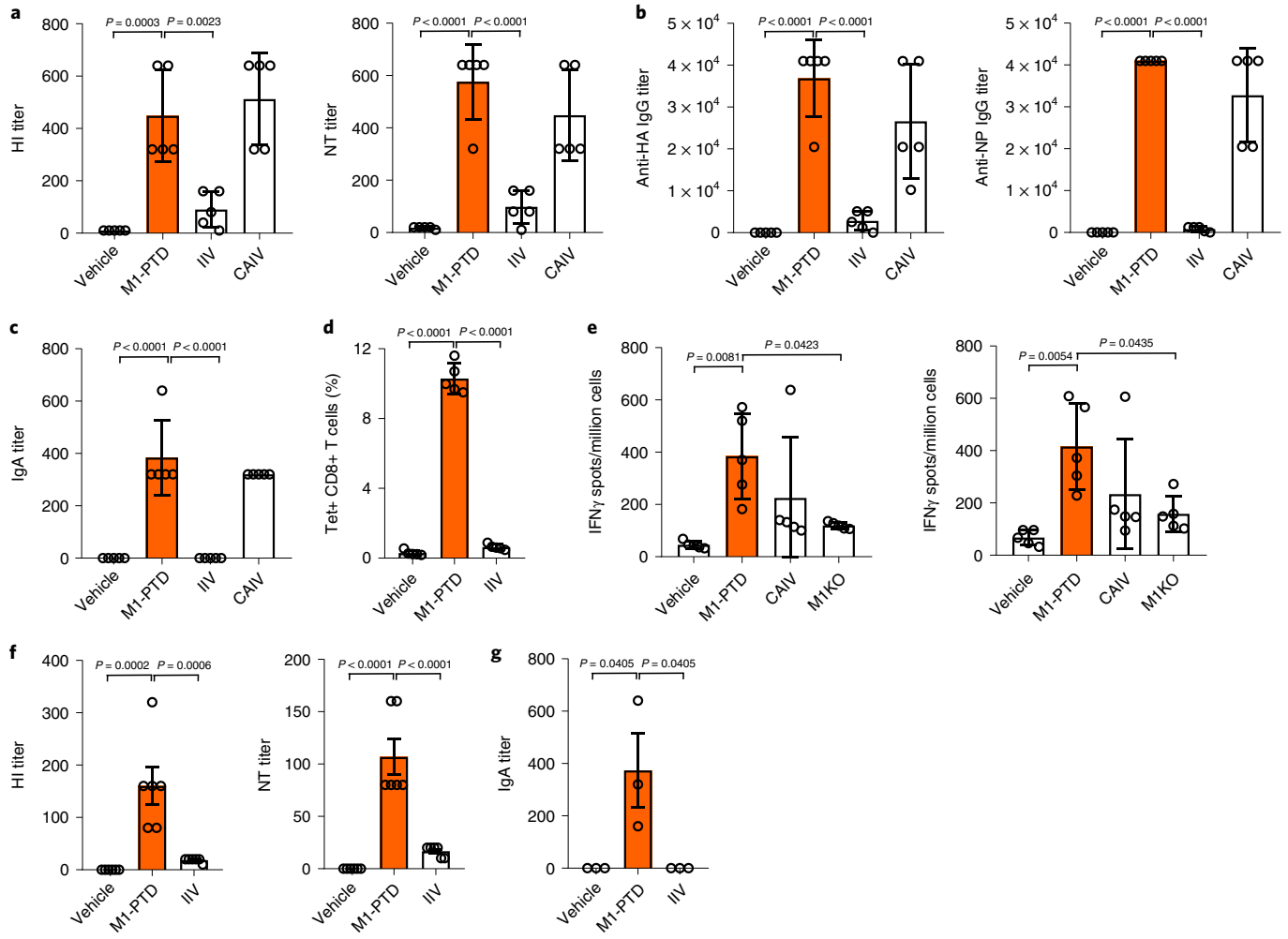

Fig. 4 | Evaluation of the immunogenicity of PROTAC virus M1-PTD in mice and ferrets. a, HI and NT antibody responses in mouse sera at day 21 after vaccination ($n = 5$). Data are plotted for individual mice and overlaid with means ± s.d.; one-way ANOVA with Tukey's multiple comparisons test. **b**, Viral surface protein HA or internal protein NP-specific IgG antibody responses in mouse sera at day 21 after vaccination ($n = 5$). Data are plotted for individual mice and overlaid with means ± s.d.; one-way ANOVA with Tukey's multiple comparisons test. **c**, Viral NP-specific mucosal IgA antibody responses in mouse lungs at day 21 after vaccination ($n = 5$). Data are plotted for individual mice and overlaid with means ± s.d.; one-way ANOVA with Tukey's multiple comparisons test. **d**, Viral NP antigen-specific CD8 T cell responses in the lungs of mice at day 21 after vaccination ($n = 5$). Data are plotted for individual mice and overlaid with means ± s.d.; one-way ANOVA with Tukey's multiple comparisons test. **e**, Viral M1 antigen-specific T cell responses in the lungs of mice measured by ELISpot assay ($n = 5$). Two M1 peptides, $M1_{128–135}$ MGLIYNRM (left) and $M1_{58–66}$ GILGFVFTL (right), were used as the stimuli. IFNγ-expressing cells per million cells are shown. Data are presented as mean ± s.d.; one-way ANOVA with Tukey's multiple comparisons test. **f**,**g**, Antibody responses in vaccinated ferrets. Female ferrets at the age of 4–6 months were inoculated with 10^6 PFU of the indicated vaccines. Three weeks after vaccination, sera were collected for detection of HI and NT antibody titers ($n = 6$) (**f**), and lungs were collected for detection of virus-specific mucosal IgA antibody titers ($n = 3$) (**g**).

~4.6-log decrease, respectively) (Fig. 3b). In the ferret model study, we further confirmed the safety of M1-PTD. By day 3 after inoculation, titers of M1-PTD in the nasal wash, trachea and lung of ferrets showed ~2.0-log, ~2.1-log and ~2.9-log decreases compared to those of WT virus, respectively (Fig. 3c). All data from the animal models indicated that influenza virus was greatly attenuated in vivo via the use of the host protein degradation machinery.

PROTAC vaccine induces robust and broad immune responses in mice and ferrets. We next tested the ability of M1-PTD to induce immune responses in mice and ferrets. In the mouse model study, M1-PTD induced dose-dependent antibody responses in the sera 3 weeks after vaccination, as measured by hemagglutinin inhibition (HI) assay, neutralization (NT) antibody assay and enzyme-linked immunosorbent assay (ELISA) (Extended Data Fig. 7a–d). The titers of HI antibodies, NT antibodies and immunoglobulin G (IgG) against viral surface HA protein and internal conserved nucleoprotein (NP) elicited by M1-PTD (10^5 PFU) were significantly (5–50-fold) higher than those elicited by the most widely used inactivated influenza vaccine (IIV) and similar to those elicited by CAIV (Fig. 4a,b). Furthermore, high levels of mucosal immune responses, indicated by secretory immunoglobulin A (IgA) antibodies against influenza virus, were elicited by M1-PTD and CAIV but not by IIV vaccination (Fig. 4c). In addition to humoral and mucosal responses, M1-PTD elicited robust T cell responses against viral NP and M1 antigens in the lungs of mice, measured by flow cytometry and enzyme-linked immunospot (ELISpot) assays, respectively (Fig. 4d,e and Extended Data Figs. 7e and 8a,b). Impressively, the viral M1 antigen-specific T cell responses elicited by M1-PTD were significantly stronger than those elicited by the replication-incompetent

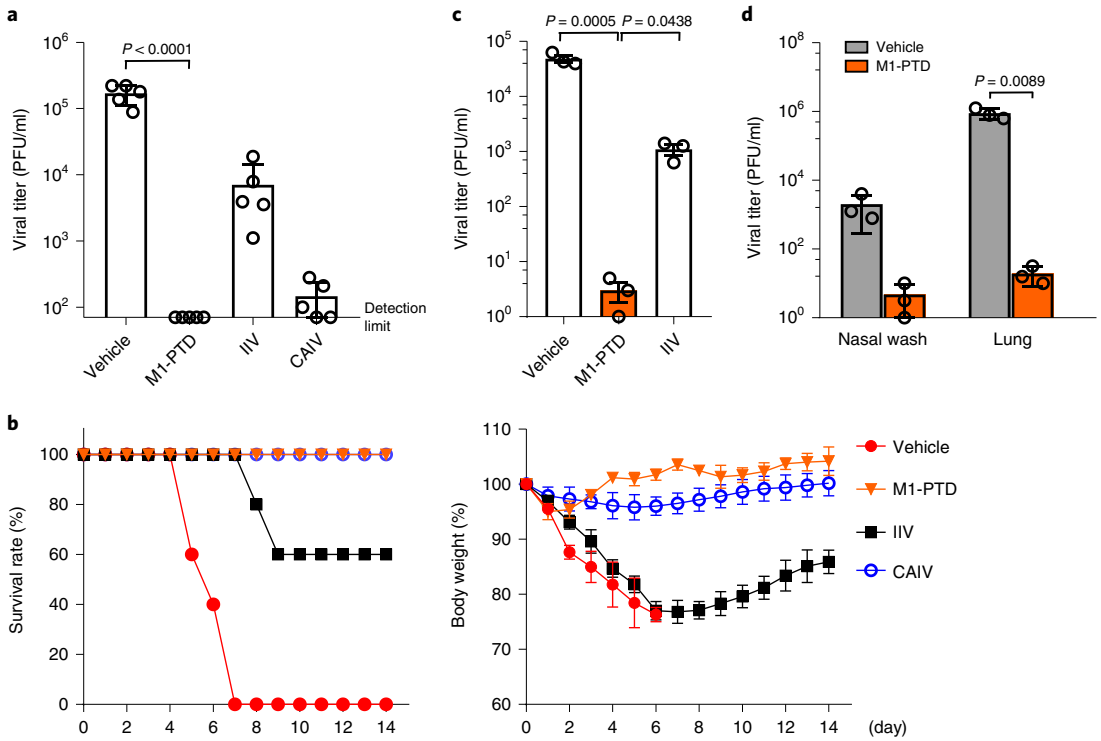

Fig. 5 | Characterizations of the protective efficacy of M1-PTD in mice and ferrets. a, Viral titers at day 3 after challenge with WT WSN virus in the lungs of mice vaccinated with the indicated vaccines ($n = 5$). Data are plotted for individual mice and overlaid with mean ± s.d.; one-way ANOVA with Tukey's multiple comparisons test. The detection limit is 70 PFU/mL. **b**, Survival rates and body weights of vaccinated mice ($n = 5$) after challenge with WT WSN virus. Data are presented as mean ± s.d. **c**, Protective efficacy of M1-PTD against homologous virus challenge in ferrets. Vaccinated ferrets with indicated vaccines were challenged with 10^7 PFU of WT WSN viruses. Lungs were collected 3 days after challenge for detection of viral titers ($n = 3$). Data are plotted for individual ferrets and overlaid with mean ± s.d.; one-way ANOVA with Tukey's multiple comparisons test. **d**, Cross-reactive protection efficacy of M1-PTD against heterologous virus challenge in ferrets. Viral titers in the nasal washes and lungs of vaccinated ferrets with 10^6 PFU of M1-PTD at day 3 after challenge with 10^6 PFU of heterologous influenza A/Netherlands/602/2009 (pdmH1N1) virus ($n = 3$). Data are plotted for individual ferrets and overlaid with mean ± s.d.; unpaired two-tailed *t*-test.

M1-deficient (M1 knockout (M1KO)) virus (Fig. 4e), which is potentially due to that PTD-mediated M1 degradation enhanced presentation of M1 peptide antigens (Extended Data Fig. 8c,d), consistent with the observations in the studies of PROTAC small chemical molecules[34,35]. In the ferret model study, M1-PTD (10^6 PFU) also elicited much stronger HI antibodies, NT antibodies and IgA antibodies than those elicited by IIV 3 weeks after vaccination (Fig. 4f,g). Our results from the animal models indicate that the PROTAC virus vaccine elicited broad and robust immunity, including humoral, mucosal and cellular responses.

PROTAC vaccine provides protection against homologous and heterologous viral challenge. We then evaluated the protective efficacy of M1-PTD against homologous and heterologous virus challenges in mice and ferrets. In the mouse model study, mice immunized with M1-PTD, IIV or CAIV were challenged with 2×10^5 PFU of WT virus 3 weeks after vaccination. To determine the inhibition of viral replication in the lungs, viral titers were analyzed 3 days after challenge. Although high viral titers were detected in mock-vaccinated mice, complete protection without detectable viral titers in the lung was achieved with a single-dose vaccination of M1-PTD at 10^5 PFU (Fig. 5a). In terms of survival rate and body weight, all mock-vaccinated mice drastically lost body weight and died by day 7 after challenge, and only 60% of IIV-vaccinated mice survived the challenge with obvious body weight loss, whereas all M1-PTD or CAIV-vaccinated mice survived the challenge and did not show any weight loss (Fig. 5b). Strong protective effects were also observed in ferrets, which were challenged 3 weeks after vaccination with 10^7 PFU of WT virus. Detection of viruses in the lungs of ferrets 3 days after challenge indicated that vaccination with M1-PTD reduced viral titers by ~4.3-log compared to mock vaccination with no clinical symptom indicative of infection, whereas vaccination with IIV reduced viral titers by only ~1.7-log (Fig. 5c). To test the protection of M1-PTD vaccination against heterologous strain, ferrets immunized with 10^6 PFU of M1-PTD were challenged with 10^6 PFU of influenza A/Netherlands/602/2009 (pdmH1N1) virus. Measurement of the viral titers 3 days after challenge indicated that M1-PTD vaccination reduced viral titers in nasal washes and lungs of ferrets by ~2.7-log and ~4.7-log, respectively, suggesting that M1-PTD vaccination provided strong heterologous protection (Fig. 5d). Such broadly cross-reactive protection resulted from the broad humoral, mucosal and cytotoxic T lymphocyte immune responses elicited by PROTAC virus vaccine against the conserved epitopes on the viral surface and internal proteins[1,15].

Finally, we tested whether this method can be applied to other influenza virus strains by incorporating PTD into M1 protein of another virus strain, influenza A/Puerto Rico/8/1934 (H1N1) virus (PR8). The resultant PROTAC virus strain, M1-PTD^{PR8}, was also highly attenuated in conventional cells as measured by CPE assay and viral replication curves (Extended Data Fig. 9), similar to the observations in M1-PTD^{WSN} virus strain (Figs. 1e,f and 2a).

Discussion

Overall, by using the host's protein degradation machinery to control viral protein stability, we successfully developed a PROTAC virus vaccine. An ideal vaccine should be sufficiently attenuated in

the host for safety while retaining robust immunogenicity for efficacy and able to be produced efficiently in manufacturing-suitable tissue culture platforms[36,37]. PROTAC virus can be highly attenuated in conventional cells but can retain the ability to replicate efficiently in the engineered TEVp-expressing MDCK cell line, which has been approved by the US Food and Drug Administration (FDA) for human vaccine production[38]. PROTAC virus can be sufficiently attenuated in vivo but can elicit robust and diverse humoral, mucosal and cellular immunity and, thus, provide broad protection against homologous and heterologous viral challenges.

In addition to the clinically used approaches to produce IIV and CAIV, several other strategies have been developed to attenuate viruses in preclinical studies[2–12]. Compared to these existing approaches, our PROTAC virus vaccine technology uses a distinct vaccine design principle—that is, conditionally targeting viral protein to the host's protein degradation system to create proteolysis-targeting virus as vaccine. Our approach has five key features. (1) This approach can highly attenuate viruses to a low level of viral replication in our experiments. Thus, PROTAC virus vaccine may have a higher level of safety than those generated by existing approaches, which still exhibit considerable replication competence in conventional cells and even kill hosts at high doses[4], leading to safety concerns. (2) It may be a useful approach to attenuate multiple circulating seasonal or pandemic virus strains, providing a sufficient antigen match between the vaccine and target virus and, thus, stronger efficacy. This contrasts with existing vaccines, such as CAIV FluMist, wherein only HA and NA are from the circulating strains, with the remaining six internal genes being from a cold-adapted master donor virus[4]. This also contrasts with mRNA vaccines, which heavily depend on delivery vehicles and mainly contain viral surface protein, usually lacking other internal conserved viral proteins that are important for the triggering of long-term cellular immunity and cross-reactive protection against heterologous viruses, although mRNA could be quickly designed and scaled up[39,40]. (3) In principle, many PTDs can be used to generate PROTAC viruses, because more than 600 E3 ligases have been found in the human ubiquitin–proteasome system (Supplementary Table 1)[27]. Given the potential dysfunction or loss of VHL in patients with VHL diseases[41], a systemic investigation on the diverse PTD–E3 ligase pairs and the linkers between PTD and viral proteins could enable the discovery of optimal PROTAC vaccine candidates with higher production efficiency, safety or efficacy that suit populations with different genetic backgrounds, such as individuals with defect or high expression levels of specific E3 ligases. In addition, the use of PROTAC vaccines for those who are receiving proteasome inhibitor therapy needs further evaluation for potential safety concerns. (4) It is a simple and general method, potentially applicable to many other viruses, and accessible to most laboratories. (5) It enables cost-effective vaccine production within weeks under normal cell culture conditions by using TEVp-expressing or viral proteins of interest-expressing cells (Extended Data Fig. 10), which is advantageous over the existing approaches that depend on embryonated eggs[15]. Therefore, this PROTAC vaccine technology could be a promising and universal strategy for creating safer and more effective vaccines against various types of viruses. The success in PROTAC vaccine technology may also represent an important breakthrough at the interface between basic research of protein degradation machinery and vaccine development, emerging as a new frontier for both areas.

Online content

Any methods, additional references, Nature Research reporting summaries, source data, extended data, supplementary information, acknowledgements, peer review information; details of author contributions and competing interests; and statements of data and code availability are available at https://doi.org/10.1038/s41587-022-01381-4.

Received: 6 January 2021; Accepted: 1 June 2022;
Published online: 4 July 2022

References

1. Yamayoshi, S. & Kawaoka, Y. Current and future influenza vaccines. *Nat. Med.* **25**, 212–220 (2019).
2. Blanco-Lobo, P., Nogales, A., Rodriguez, L. & Martinez-Sobrido, L. Novel approaches for the development of live attenuated influenza vaccines. *Viruses* **11**, 190 (2019).
3. Coleman, J. R. et al. Virus attenuation by genome-scale changes in codon pair bias. *Science* **320**, 1784–1787 (2008).
4. Mueller, S. et al. Live attenuated influenza virus vaccines by computer-aided rational design. *Nat. Biotechnol.* **28**, 723–726 (2010).
5. Si, L. et al. Generation of influenza A viruses as live but replication-incompetent virus vaccines. *Science* **354**, 1170–1173 (2016).
6. Du, Y. et al. Genome-wide identification of interferon-sensitive mutations enables influenza vaccine design. *Science* **359**, 290–296 (2018).
7. Talon, J. et al. Influenza A and B viruses expressing altered NS1 proteins: a vaccine approach. *Proc. Natl Acad. Sci. USA* **97**, 4309–4314 (2000).
8. Mossler, C. et al. Phase I/II trial of a replication-deficient trivalent influenza virus vaccine lacking NS1. *Vaccine* **31**, 6194–6200 (2013).
9. Steel, J. et al. Live attenuated influenza viruses containing NS1 truncations as vaccine candidates against H5N1 highly pathogenic avian influenza. *J. Virol.* **83**, 1742–1753 (2009).
10. Wu, C. Y. et al. Influenza A surface glycosylation and vaccine design. *Proc. Natl Acad. Sci. USA* **114**, 280–285 (2017).
11. Wang, L. et al. Generation of a live attenuated influenza vaccine that elicits broad protection in mice and ferrets. *Cell Host Microbe* **21**, 334–343 (2017).
12. Jung, E. J., Lee, K. H. & Seong, B. L. Reverse genetic platform for inactivated and live-attenuated influenza vaccine. *Exp. Mol. Med.* **42**, 116–121 (2010).
13. Krammer, F. & Palese, P. Advances in the development of influenza virus vaccines. *Nat. Rev. Drug Discov.* **14**, 167–182 (2015).
14. Ulmer, J. B., Valley, U. & Rappuoli, R. Vaccine manufacturing: challenges and solutions. *Nat. Biotechnol.* **24**, 1377–1383 (2006).
15. Wei, C. J. et al. Next-generation influenza vaccines: opportunities and challenges. *Nat. Rev. Drug Discov.* **19**, 239–252 (2020).
16. Gouma, S., Anderson, E. M. & Hensley, S. E. Challenges of making effective influenza vaccines. *Annu. Rev. Virol.* **7**, 495–512 (2020).
17. Moeller, A., Kirchdoerfer, R. N., Potter, C. S., Carragher, B. & Wilson, I. A. Organization of the influenza virus replication machinery. *Science* **338**, 1631–1634 (2012).
18. Scudellari, M. Protein-slaying drugs could be the next blockbuster therapies. *Nature* **567**, 298–300 (2019).
19. Salami, J. & Crews, C. M. Waste disposal—an attractive strategy for cancer therapy. *Science* **355**, 1163–1167 (2017).
20. Cromm, P. M. & Crews, C. M. Targeted protein degradation: from chemical biology to drug discovery. *Cell Chem. Biol.* **24**, 1181–1190 (2017).
21. Deshaies, R. J. Protein degradation: prime time for PROTACs. *Nat. Chem. Biol.* **11**, 634–635 (2015).
22. Yau, R. & Rape, M. The increasing complexity of the ubiquitin code. *Nat. Cell Biol.* **18**, 579–586 (2016).
23. Finley, D. Recognition and processing of ubiquitin–protein conjugates by the proteasome. *Annu. Rev. Biochem.* **78**, 477–513 (2009).
24. Hon, W. C. et al. Structural basis for the recognition of hydroxyproline in HIF-1α by pVHL. *Nature* **417**, 975–978 (2002).
25. Jaakkola, P. et al. Targeting of HIF-α to the von Hippel–Lindau ubiquitylation complex by O_2-regulated prolyl hydroxylation. *Science* **292**, 468–472 (2001).
26. Ivan, M. et al. HIFα targeted for VHL-mediated destruction by proline hydroxylation: implications for O_2 sensing. *Science* **292**, 464–468 (2001).
27. Gu, S., Cui, D., Chen, X., Xiong, X. & Zhao, Y. PROTACs: an emerging targeting technique for protein degradation in drug discovery. *Bioessays* **40**, e1700247 (2018).
28. Zhang, C. et al. USP9X destabilizes pVHL and promotes cell proliferation. *Oncotarget* **7**, 60519–60534 (2016).
29. Latif, F. et al. Identification of the von Hippel–Lindau disease tumor suppressor gene. *Science* **260**, 1317–1320 (1993).
30. Iwai, K. et al. Identification of the von Hippel–Lindau tumor-suppressor protein as part of an active E3 ubiquitin ligase complex. *Proc. Natl Acad. Sci. USA* **96**, 12436–12441 (1999).
31. Los, M. et al. Expression pattern of the von Hippel–Lindau protein in human tissues. *Lab. Invest.* **75**, 231–238 (1996).
32. Yang, J. et al. The I-TASSER Suite: protein structure and function prediction. *Nat. Methods* **12**, 7–8 (2015).
33. Broadbent, A. J., Santos, C. P., Godbout, R. A. & Subbarao, K. The temperature-sensitive and attenuation phenotypes conferred by mutations in the influenza virus PB2, PB1, and NP genes are influenced by the species of origin of the PB2 gene in reassortant viruses derived from influenza A/California/07/2009 and A/WSN/33 viruses. *J. Virol.* **88**, 12339–12347 (2014).

34. Jensen, S. M., Potts, G. K., Ready, D. B. & Patterson, M. J. Specific MHC-I peptides are induced using PROTACs. *Front. Immunol.* **9**, 2697 (2018).
35. Moser, S. C., Voerman, J. S. A., Buckley, D. L., Winter, G. E. & Schliehe, C. Acute pharmacologic degradation of a stable antigen enhances its direct presentation on MHC class I molecules. *Front. Immunol.* **8**, 1920 (2017).
36. Hussain, A. I., Cordeiro, M., Sevilla, E. & Liu, J. Comparison of egg and high yielding MDCK cell-derived live attenuated influenza virus for commercial production of trivalent influenza vaccine: in vitro cell susceptibility and influenza virus replication kinetics in permissive and semi-permissive cells. *Vaccine* **28**, 3848–3855 (2010).
37. Pica, N. & Palese, P. Toward a universal influenza virus vaccine: prospects and challenges. *Annu. Rev. Med.* **64**, 189–202 (2013).
38. Ping, J., Lopes, T. J., Neumann, G. & Kawaoka, Y. Development of high-yield influenza B virus vaccine viruses. *Proc. Natl Acad. Sci. USA* **113**, E8296–E8305 (2016).
39. Dolgin, E. mRNA flu shots move into trials. *Nat. Rev. Drug Discov.* **20**, 801–803 (2021).
40. Lowe, D. Moderna's mRNA flu vaccine. *Science* https://www.science.org/content/blog-post/moderna-s-mrna-flu-vaccine (2021).
41. Gossage, L., Eisen, T. & Maher, E. R. VHL, the story of a tumour suppressor gene. *Nat. Rev. Cancer* **15**, 55–64 (2015).

Methods

Viruses, cells and vaccines. Influenza A/WSN/33 (H1N1) virus (WSN) and influenza A/Puerto Rico/8/1934 (H1N1) virus (PR8) were used as study models. Influenza A/Netherlands/602/2009 virus (pdmH1N1) was kindly provided by Ron A. M. Fouchier from the National Influenza Center and Department of Virology, Erasmus Medical Center, Rotterdam, Netherlands. WSN and pdmH1N1 viruses were used for the challenge experiments in mice and ferrets. HEK293T (CRL-3216) and MDCK.2 (CRL-2936) cell lines were obtained from the American Type Culture Collection and cultured in DMEM (Gibco, 10569-010 or c11995500BT) supplemented with 10% FBS (Gibco, 10082-147, or PAN, ST30-3302), 100 μg ml^{-1} of streptomycin and 100 U ml^{-1} of penicillin at 37 °C in 5% CO_2. MDCK.2 is a standard cell line in the field of influenza virus and vaccine research and has been approved by the FDA for human vaccine production[42]. Raw264.7 cell line was kindly provided by Tianhui Hu from the Cancer Research Center of Xiamen University and cultured in DMEM (Gibco, c11995500BT) supplemented with 10% FBS (PAN, ST30-3302), 100 μg ml^{-1} of streptomycin and 100 U ml^{-1} of penicillin at 37 °C in 5% CO_2. The clinically used approaches were used to generate the most widely used IIV and CAIV as positive controls[6,33,43,44]. To generate IIV, WSN influenza virus-containing culture supernatants were treated with 0.1–0.2% formalin (Sigma-Aldrich) at 4 °C for 1 week. After confirmation of viral inactivation by the absence of detectable infectious virus in MDCK.2 cells, the formalin-inactivated virus was purified by sucrose gradient ultracentrifugation and quantified for concentration of HA by ELISA[43,44]. The doses of IIV and PROTAC vaccine used in animal experiments were unified by the same amount of HA. To generate CAIV, five cold-adapted mutations from clinically used influenza vaccine FluMist were incorporated into three gene segments of WSN influenza virus: 265S in PB2; 391E, 581G and 661T in PB1; and 34G in NP[6,33]. CAIV was validated by the temperature-sensitive and attenuation phenotypes as described previously[6,33]. A replication-incompetent M1-deficient virus (M1KO) was also generated by introducing a stop codon at P16 of M1 protein of WSN influenza virus and propagating this virus in M1-expressing HEK293T cells, as described previously with modifications[45].

Plasmid construction. The 12-plasmid influenza A/WSN/33 (H1N1) virus rescue system[46] and the eight-plasmid influenza A/PR8/34 (H1N1) virus rescue system[47] were kindly provided by George F. Gao from the Center for Molecular Virology, CAS Key Laboratory of Pathogenic Microbiology and Immunology, Institute of Microbiology, Chinese Academy of Sciences, and Xavier Saelens from the VIB-UGent Center for Medical Biotechnology. Engineered plasmids containing cleavable PTD within the open reading frame were obtained from the WT plasmids via mutagenesis (Agilent Technologies) and confirmed by gene sequencing (TsingKe Beijing). The lentiviral vector (lenti-TEVp) used to generate the TEVp-expressing stable cell lines was a gift from Marco Tripodi. The helper plasmids (psPAX2 and pMD2G-VSVG) were kindly provided from Corregene Biotechnology. All plasmids used for transfection were amplified using a PureYield Plasmid Maxiprep Kit (Promega), according to the manufacturer's instructions.

Antibodies. Anti-M1 antibody (40010-RP01, 1:1,000 dilution for western blotting, 1:400 for immunofluorescence staining, 1:100 dilution for flow cytometry) was purchased from Sino Biological. Rabbit anti-M1 peptide (MGLIYNRM) antibody (1:100 dilution for flow cytometry) was customized and validated by Sino Biological. Anti-M1 antibody (NBP2-14995, 1:1,000 dilution for western blotting, 1:200 dilution for immunofluorescence staining) was purchased from Novus Biologicals. Anti-M1 antibody (ab25918, 1:1,000 dilution for western blotting), anti-NP (ab128193, 1:200 dilution for immunofluorescence staining), anti-HIF1α (ab179483, 1:500 dilution) and anti-rabbit IgG-HRP (ab6721, 1:2,000 dilution) were purchased from Abcam. Anti-TEVp antibody (NBP1-97669, 1:500 dilution) was purchased from Novus Biologicals. Anti-TEVp antibody (PAB19931, 1:500 dilution) was purchased from Abnova. Anti-β-tubulin antibody (700608, 1:10,000 dilution) was purchased from Zen Bio. Anti-VHL antibody (GTX101087, 1:1,000 dilution for western blotting, 1:100 dilution for immunofluorescence staining and immunohistochemistry staining) and anti-GAPDH antibody (GTX100118, 1:5,000 dilution) were purchased from GeneTex. Anti-rabbit IgG-HRP (7074S, 1:4,000 dilution) was purchased from Cell Signaling Technology. Anti-rabbit IgG-HRP (SA00001-2, 1:2,000 dilution) and anti-mouse IgG-HRP (SA00001-1, 1:2,000 dilution) were purchased from Proteintech. Alexa Fluor 488 goat anti-mouse IgG (A11001, 1:1,000 dilution) and Alexa Fluor 488 goat anti-rabbit IgG (A11034, 1:1,000 dilution for immunofluorescence staining, 1:500 dilution for flow cytometry) were purchased from Life Technologies. APC anti-mouse CD8a antibody (100712, 1:100 dilution) and APC anti-mouse CD4 antibody (100412, 1:125 dilution) were purchased from BioLegend. Anti-mouse CD8a-FITC antibody (553031, 1:100 dilution) was purchased from BD Biosciences. HRP-conjugated anti-mouse IgA antibody (ab97235, 1:2,000 dilution) was purchased from Abcam. HRP-conjugated anti-ferret IgA antibody (618-103-006, 1:2,000 dilution) was purchased from Rockland Immunochemicals.

Establishment of stable cell lines HEK293T-TEVp and MDCK-TEVp. In total, 1×10^8 HEK293T cells were seeded into a 15-cm dish in DMEM medium (Gibco, without sodium pyruvate) supplemented with 10% FBS (Gibco) 24 hours before transfection. Then, a mixture of 15 μg of lenti-TEVp plasmid, 9 μg of psPAX2 and 6 μg of pMD2G-VSVG was transfected into the cells using TransIT-X2 Dynamic Delivery System (Mirus), according to the manufacturer's instructions. Six hours later, the transfection medium was replaced by DMEM (Gibco, with sodium pyruvate) supplemented with 3% FBS. The lentivirus-containing supernatant was harvested 48 hours after transfection and filtered through a 0.45-μm filter. Then, stable lentiviral transduction was performed to integrate the TEVp gene into the genome of HEK293T and MDCK.2 cells. HEK293T or MDCK.2 cells were seeded in a six-well plate and transduced 24 hours later with lentiviral filtrates in the presence of 8 μg ml^{-1} of polybrene. Then, selection was performed under the pressure of 2 μg ml^{-1} of puromycin (InvivoGen, ani-pr) until parental cells completely died. The resultant stably transduced cells were subjected to monoclonal culture by inoculating into a 96-well plate. The HEK293T-TEVp and MDCK-TEVp cells with the highest TEVp expression levels were selected for influenza virus generation.

qRT–PCR. Cells were collected and RNA was extracted by QIAamp Viral RNA Mini Kit (QIAGEN, 52906) and reverse transcribed into cDNA by using Reverse Transcription System (Promega, A3500), according to the manufacturers' instructions. Absolute quantification of copy numbers of TEVp mRNA in cells was performed using GoTaq qPCR Master Mix (Promega, A6001), according to the manufacturer's instructions. Lenti-TEVp plasmid was used as standard DNA to obtain the standard curve. The forward and reverse primers for TEVp were TCATTACAAACAAGCACTTG and TAGGCATGCGAATAATTATC, respectively. The forward and reverse primers for viral NP were TCAAGTGAGA GAGAGCCGGA and TCAAAGTCGTACCCACTGGC, respectively. The PCR conditions were one cycle at 95 °C for 5 minutes; 40 cycles at 95 °C for 15 seconds and 60 °C for 20 seconds; and one cycle at 95 °C for 15 seconds, 60 °C for 15 seconds and 95 °C for 15 seconds. The data were analyzed according to the manufacturer's instructions.

Western blotting. Total protein concentrations of cell lysates were determined by Pierce BCA kit (Thermo Fisher Scientific). Lysates were separated on FuturePAGE 4–12% tris-glycine gels (ACE, F11412Gel) or Novex WedgeWell 4–20% tris-glycine gels (Invitrogen, XP04200BOX) and transferred onto PVDF membranes (Invitrogen, IB24001, or Millipore, IPVH00010). Membranes were blocked with 5% non-fat milk (YEASEN, 36120ES76, or BD Biosciences, 232100) in TBST (0.1% Tween-20 in tris-buffered saline) (Coolaber, SL1328-500mL×10, or Abcam, ab64204) before overnight incubation with indicated antibodies. After incubation with the appropriate HRP-conjugated secondary antibodies, the bands were visualized by chemiluminescence (Pierce West Femto ECL).

Generation of WT influenza viruses and PROTAC influenza viruses harboring cleavable PTD(s) in their genome. For generation of WT WSN influenza virus, 2×10^5 cells per well from the HEK293T-TEVp cell line under passage 15 and 5×10^4 cells per well from the MDCK-TEVp cell line under passage 15 were seeded into six-well plates in DMEM (Gibco) supplemented with 10% FBS (Gibco) and 2 μg ml^{-1} of puromycin (InvivoGen, ant-pr). The co-culture of HEK293T and MDCK.2 cells is a standard method to generate influenza viruses: HEK293T cells enable highly efficient transfection of plasmids for the first round of virus production, whereas MDCK.2 cells further expand the progeny viruses to higher titers[48]. Twenty-four hours later, a mixture of 0.2 μg each of the plasmids in the virus rescue system was transfected into the HEK293T-TEVp/MDCK-TEVp co-culture using TransIT-X2 Dynamic Delivery System (Mirus, MIR 6003), according to the manufacturer's instructions. After 6 hours, the transfection medium was replaced with DMEM supplemented with 0.5% FBS and 2 μg ml^{-1} of L-1-tosylamide-2-phenylethyl chloromethyl ketone (TPCK)-treated trypsin (Sigma-Aldrich). The cells were further cultured for 4 days at 37 °C in 5% CO_2, and then the supernatant was collected. The virus in the supernatant was amplified in MDCK-TEVp cells in DMEM supplemented with 0.5% FBS and 2 μg ml^{-1} of TPCK-treated trypsin. The supernatant containing the generated virus was harvested and centrifuged at 1,000*g* for 10 minutes to remove cell debris. To generate PROTAC influenza viruses, an almost identical procedure was carried out with the following modification: the plasmid-expressing WT viral RNA was replaced by the corresponding engineered plasmid harboring cleavable PTD within the open reading frame.

For generation of WT PR8 influenza virus, 2×10^5 cells per well from the HEK293T-TEVp cell line under passage 15 and 10^5 cells per well from the MDCK-TEVp cell line under passage 15 were seeded into six-well plates in DMEM supplemented with 10% FBS (Gibco) and 2 μg ml^{-1} of puromycin (InvivoGen, ant-pr). Twenty-four hours later, cell culture medium was replaced with Opti-MEM (Gibco, 31985-070), and a mixture of 0.4 μg each of the plasmids in the virus rescue system was transfected into the HEK293T-TEVp/MDCK-TEVp co-culture using TransIT-X2 Dynamic Delivery System (Mirus, MIR 6003), according to the manufacturer's instructions. After 6 hours, the transfection medium was replaced with Opti-MEM. Twenty-four hours after transfection, cell culture was supplemented with 0.5 μg ml^{-1} of TPCK-trypsin. The cells were further cultured for 4–5 days at 37 °C in 5% CO_2, and then the supernatant was collected. The virus in the supernatant was amplified in MDCK-TEVp cells

in Opti-MEM supplemented with 0.5 μg ml^{-1} of TPCK-treated trypsin. The supernatant containing the generated virus was harvested and centrifuged at 1,000*g* for 10 minutes to remove cell debris. To generate PROTAC influenza virus, an almost identical procedure was carried out with the following modification: the plasmid-expressing WT viral RNA was replaced by the corresponding engineered plasmid harboring cleavable PTD within the open reading frame.

CPE assay. Cells were seeded into six-well or 96-well plates, cultured for 24 hours and incubated with influenza viruses in DMEM supplemented with 0.5% FBS and 2 μg ml^{-1} of TPCK-treated trypsin. After 4–5 days of incubation, CPE was observed and recorded under microscope. The CPE was precisely quantified by CellTiter-Glo assay, a standard method of determining the number of viable cells. In brief, CellTiter-Glo reagent (Promega) was added to each well, and the plates were read using a plate reader, according to the manufacturer's instructions.

Plaque formation assay. MDCK.2 cells or MDCK-TEVp cells were seeded in a 12-well plate to produce a confluent monolayer. The next day, the cells were washed with PBS and infected with a ten-fold dilution series of the virus in DMEM medium, in a total volume of 1 ml. The inoculum was removed after 1 hour of incubation at 37 °C and replaced by 1 ml of DMEM supplemented with 1.5% low-melting-point agarose (Amresco, 0815-100G) and 2 μg ml^{-1} of TPCK-treated trypsin. After 4–5 days of incubation at 37 °C in 5% CO_2, the cells were fixed with 4% paraformaldehyde (PFA) and then stained with crystal violet (Sigma-Aldrich). Visible plaques were counted, and the virus titers were determined.

$TCID_{50}$ assay. MDCK.2 cells or MDCK-TEVp cells were seeded in 96-well plates at 5,000 cells per well. Twenty-four hours later, cell culture medium was removed, and cells were infected with ten-fold serial dilutions of viral supernatants starting at 1:10 in DMEM supplemented with 0.5% FBS and 2 μg ml^{-1} of TPCK-trypsin. The assay was carried out in eight parallels with the last column of the 96-well plate as cell control without virus. After 4–5 days of incubation at 37 °C in 5% CO_2, the cells were fixed with 4% PFA and then stained with crystal violet (Sigma-Aldrich). The percentage of CPE was recorded for each virus dilution, and the $TCID_{50}$ per milliliter ($TCID_{50}$/ml) for given virus was calculated according to the Reed–Muench method[49]. The viral titers were expressed as PFU/mL by multiplying the $TCID_{50}$/ml by 0.7 (ref. [50]).

Virus growth kinetics analysis. To determine in vitro virus growth kinetics, 15–20 × 10^4 cells per well from MDCK-TEVp cell line or MDCK.2 cell line were seeded into six-well plates in DMEM supplemented with 10% FBS. Twenty-four hours later, the cells were infected with an MOI = 0.01 of viruses for 1 hour at 37 °C. After washing with PBS, the cells were further cultured in DMEM supplemented with 0.5% FBS and 2 μg ml^{-1} of TPCK-treated trypsin. At the indicated times after infection (24, 48, 72 and 96 hours), the cell supernatants were collected, and viral titers were determined by the plaque formation assay and $TCID_{50}$ assay as described above.

Immunofluorescence assay. Influenza virus propagation in TEVp-expressing stable cells and conventional cells was determined by immunofluorescence. Then, 10^5 cells per well from MDCK-TEVp cell line or MDCK.2 cell line were seeded into 12-well plates in DMEM supplemented with 10% FBS. Twenty-four hours later, the cells were infected with an MOI = 0.01 of viruses in DMEM supplemented with 0.5% FBS and 2 μg ml^{-1} of TPCK-treated trypsin. To confirm that the live attenuation of the PROTAC viruses was proteasome dependent, a parallel experiment was conducted, in which the culture medium was supplemented with indicated concentrations of proteasome inhibitor MG-132 (Sigma-Aldrich, M7449-1mL). Forty-eight hours after infection, the cells were fixed with 4% PFA, permeabilized with 0.1% Triton X-100 in PBS (PBST) and blocked with 10% goat serum in PBST. Anti-M1 antibody (Novus Biologicals, NBP2-14995, or Sino Biological, 40010-RP01) or anti-NP antibody (Abcam, ab128193) was used to detect influenza viral M1 or NP protein, respectively. Alexa Fluor 488 goat anti-rabbit IgG (Life Technologies) or Alexa Fluor 488 goat anti-mouse IgG (Life Technologies) was used as secondary antibody. Cell nuclei were visualized with DAPI (Invitrogen). Images were recorded with a fluorescence microscope (Nikon), and image processing was done using NIS-Elements (Nikon). Virus infection was quantified by measuring the percentages of M1-positive or NP-positive cells in 3–5 different fields for each condition.

Genetic stability evaluation of PROTAC influenza viruses. MDCK-TEVp cells at 5 × 10^4 cells per well in 24-well plates were infected with PROTAC influenza virus strains at an MOI of 0.01 in DMEM supplemented with 0.5% FBS and 2 μg ml^{-1} of TPCK-treated trypsin. When >90% CPE was observed, the supernatants were harvested and used for infection in the next round of investigation. The procedure was repeated more than 20 times. Influenza viral RNA was extracted by using QIAamp Viral RNA Mini Kit (QIAGEN) and reverse transcribed into cDNA by using Reverse Transcription System (Promega), according to the manufacturer's instructions. The resultant cDNA products were subjected to sequencing to investigate whether any mutation occurred during virus propagation.

Concentration and purification of influenza virus particles. Influenza viruses were produced as described above. The virus-containing supernatant was harvested and centrifuged at 10^3*g* for 15 minutes at 4 °C to remove cell debris. Then, the supernatant was collected and concentrated by ultracentrifugation at 10^5*g* for 2 hours at 4 °C in a Ti40 rotor. The resultant virus precipitation was resuspended in 500 μl of buffer containing 100 mM NaCl, 10 mM Tris-Cl (pH 7.4) and 1 mM EDTA and purified by density gradient centrifugation of sucrose (20–60%) at 10^5*g* for 2 hours at 4 °C in a SW40 rotor. The banded viruses were collected, diluted with buffer containing 100 mM NaCl, 10 mM Tris-Cl (pH 7.4) and 1 mM EDTA, pelleted by centrifugation at 10^5*g* for 2 hours at 4 °C in a SW40 rotor and resuspended in PBS. The purified viruses were either used immediately or stored at −80 °C until use. The influenza virus particles could also be concentrated and purified using PEGeasy Virus Concentration Reagent (DongLing Biotech, GE-19002-50), according to the manufacturer's instructions with some modifications. In brief, the virus-containing supernatant was harvested and centrifuged at 3,200*g* for 15 minutes at 4 °C to remove cell debris. Then, the supernatant was collected and incubated with PEG solution overnight at 4 °C and centrifuged at 3,200*g* for 30 minutes at 4 °C. The resultant virus precipitation was resuspended in PBS and either used immediately or stored at −80 °C until use.

Mouse studies. Female specific-pathogen-free BALB/c, C57BL/6J and BALB/c nude mice (Vital River Laboratory Animal Technology and GemPharmatech) at the age of 6–8 weeks were used to evaluate safety, immunogenicity and protection efficacy of vaccines. Housing conditions were: 12-hour light/dark cycle, 24 °C and 50% humidity. The LD_{50} of WT WSN virus in BALB/c mice was determined to be approximately 10^4 PFU.

To measure viral replicative capacity, groups of 15 BALB/c mice were anesthetized with tribromoethanol and intranasally inoculated with 50 μl of 10^4 or 10^5 PFU of WT WSN, 10^4 or 10^5 PFU of PROTAC virus M1-PTD or DMEM as a control. To quantify viral replication in mouse, five mice from each group were sacrificed at day 3 after infection, and their organs were harvested, homogenized and freeze–thawed three times to release the virus, which was titered by plaque formation assay and $TCID_{50}$ assay. The remaining ten mice were monitored daily for body weight loss and death for 14 days.

To test the dose-dependent antibody responses elicited by M1-PTD, groups of five BALB/c mice were anesthetized with tribromoethanol and intranasally inoculated with 50 μl of 10^2, 10^3, 10^4 or 10^5 PFU of M1-PTD or with DMEM as a control. Sera samples were collected at day 21 after vaccination and subjected to IgG antibody detection, HI assay and NT assay.

To explore the effects of T cell deficiency on the antibody responses elicited by M1-PTD, groups of five BALB/c nude mice were anesthetized with tribromoethanol and intranasally inoculated with 50 μl of 10^4 PFU of M1-PTD or DMEM. Sera samples were collected at day 21 after vaccination and subjected to IgG antibody detection, HI assay and NT assay.

To test the dose-dependent T cell responses elicited by M1-PTD, groups of five C57BL/6J mice were anesthetized with tribromoethanol and intranasally inoculated with 50 μl of 10^2, 10^3, 10^4 or 10^5 PFU of M1-PTD or with DMEM as a control. Mouse lung tissue samples were harvested at day 8 after vaccination and used for detection of viral M1 peptide-specific T cell responses by IFN-γ ELISpot assay.

To evaluate the immunogenicity and protection efficacy of M1-PTD, IIV and CAIV, groups of 15 mice were anesthetized with tribromoethanol and intranasally inoculated with 50 μl of 10^5 PFU of M1-PTD or CAIV or intramuscularly inoculated with the same dosage of IIV. Sera samples and bronchoalveolar lavage (BAL) samples were collected from five animals in each group at day 21 after vaccination and subjected to IgG antibody detection, HI assay, NT assay and IgA detection, respectively. At day 21 after vaccination, groups of ten mice were anesthetized with tribromoethanol and intranasally challenged with 2 × 10^5 PFU of WT WSN viruses. At day 3 after challenge, five mice from each group were sacrificed, and their lung organs were collected for quantification of virus titers by $TCID_{50}$ and plaque formation assay. The remaining five mice were monitored daily for body weight loss and death for 14 days.

To evaluate the ability of M1-PTD, IIV, CAIV and M1KO to induce T cell responses, groups of five C57BL/6J mice were anesthetized with tribromoethanol and intranasally inoculated with 50 μl of 10^5 PFU of M1-PTD, CAIV or M1KO or intramuscularly inoculated with the same dosage of IIV. Mouse lung tissue samples were harvested at day 8 after vaccination and used for detection of $CD8^+$ T cells, $CD4^+$ T cells and viral NP peptide-specific $CD8^+$ T cells by flow cytometry or viral M1 peptide-specific T cell responses by IFN-γ ELISpot assay.

Ferret studies. Female seronegative ferrets (Wuxi Cay Ferret Farm) at the age of 4–6 months were used to evaluate safety, immunogenicity and protection efficacy of vaccines.

To evaluate the replication of WT WSN and PROTAC virus, groups of three ferrets were intranasally inoculated with 500 μl of 10^5 PFU of WT WSN or M1-PTD or with PBS as a control. At day 3 after inoculation, ferrets from each group were sacrificed, and their organs were harvested for virus titer detection by plaque formation assay.

To evaluate the immunogenicity and protective efficacy, groups of six ferrets were intranasally inoculated with 500 µl of 10^6 PFU of M1-PTD or PBS or intramuscularly inoculated with the same dosage of IIV. At day 21 after vaccination, sera samples were collected from six ferrets in each group and subjected to HI and NT assays, and lung tissue samples were harvested from three ferrets in each group for detection of IgA. The remaining three ferrets were intranasally challenged with 10^7 PFU of WT WSN viruses. At day 3 after challenge, three ferrets from each group were sacrificed, and their organs were collected for quantification of virus titers by plaque formation assay.

To evaluate cross-protection from heterologous influenza virus challenge, groups of three ferrets were intranasally inoculated with 500 µl of 10^6 PFU of either M1-PTD1 or PBS. At day 21 after vaccination, the ferrets were challenged with 10^6 PFU of heterologous influenza A/Netherlands/602/2009 (pdmH1N1) viruses. At day 3 after challenge, nasal washes and organs were collected from three ferrets in each group for quantification of virus titers by plaque formation assay.

Animal experiments were performed in accordance with the guidelines of the Institutional Animal Care and Use Committees of Shenzhen Institute of Advanced Technology, the Chinese Academy of Sciences, Sinovac Biotech, Servicebio and Peking University.

Informed consent was obtained from all participants in the study. The use of paraffin-embedded and frozen sections of human lung tissue was in accordance with all relevant ethical regulations and approved by the Ethics Committee of West China Hospital of Sichuan University.

HI assay. The titers of HI antibodies in sera samples were tested by a standard HI assay[5]. In brief, receptor-destroying enzyme (RDE)-incubated sera samples were pre-treated for 30 minutes at 56 °C. Sera samples were two-fold serially diluted starting at 1:10 in PBS in a V-shaped 96-well plate and incubated with four HA units of WT virus for 1 hour at 37 °C. Then, 0.5% (v/v) chicken red blood cells in PBS were added to each well and incubated for 30 minutes at room temperature. The HI titers were read as the highest dilution of sera samples that inhibited hemagglutination.

Virus NT assay. MDCK.2 cells were seeded into 96-well plates in DMEM supplemented with 10% FBS to produce a confluent monolayer. RDE-treated sera samples were two-fold serially diluted starting at 1:10 in DMEM supplemented with 1% FBS and incubated with virus (MOI = 0.01) for 1 hour at 37 °C. Then, the sera/virus mixture was applied to MDCK.2 cells in DMEM supplemented with 1% FBS and 2 µg ml^{-1} of TPCK-treated trypsin and incubated for 3–5 days at 37 °C in 5% CO_2. CPE was observed and recorded. Antibody neutralizing titers were read as the reciprocals of the highest dilution of sera samples that completely inhibited CPE.

ELISA. ELISA was used to analyze IgG antibody in sera and IgA antibody in BAL samples from the immunized animals. Recombinant proteins (HA and NP) of WT viruses (1 µg ml^{-1}) (Sino Biological, 11692-V08H for HA and 11675-V08B for NP) were diluted in ELISA coating buffer (Solarbio, C1055). Then, 50 µl of this solution was added to the wells of a 96-well ELISA microplate (Corning, 3590) and incubated overnight at 4 °C. After washing three times with washing buffer (PBS containing 0.1% Tween 20), 100 µl of blocking buffer (5% non-fat milk (YEASEN, 36120ES60) in washing buffer) was applied to all wells for 1 hour at 37 °C. After removing the blocking buffer and washing three times with washing buffer, 100 µl of serum or BAL samples diluted in blocking buffer was added to each well, and the plate was incubated for 2 hours at 37 °C. After washing three times with washing buffer, 100 µl of HRP-conjugated anti-mouse IgG antibody (Proteintech) or HRP-conjugated anti-mouse/ferret IgA antibody (Abcam/Rockland Immunochemicals) diluted in blocking buffer was applied to each well for 1.5 hours at 37 °C. After washing five times with washing buffer, microplates were detected with 100 µl of 3,3′,5,5′-tetramethyl benzidine (TMB) substrate (Beyotime, P0209), and the reaction was stopped after 15 minutes by the addition of 100 µl of ELISA stop solution (Solarbio, C1058). The spectroscopic absorbance of each well was read by an automated plate reader (BioTek Synergy H1) at a wavelength of 450 nm.

Analysis of influenza virus-induced T cell responses by flow cytometry. Tetramer staining and flow cytometry were used to detect influenza virus NP-specific $CD8^+$ T cells[5,6]. In brief, mouse lung tissues were harvested, and single-cell suspensions were generated. T cell population was enriched using the EasySep Mouse T Cell Isolation Kit (STEMCELL Technologies) and stained with anti-mouse CD8a-FITC antibody (BD Biosciences) and phycoerythrin-conjugated H-2D^b tetramer specific to influenza viral NP epitope ($NP_{366–374}$, ASNENMETM) (MBL). To detect $CD8^+$ and $CD4^+$ T cells, the single-cell suspensions were strained with APC anti-mouse CD8a antibody (BioLegend) or APC anti-mouse CD4 antibody (BioLegend), respectively. Samples were analyzed with a fluorescence-activated cell sorting (FACS) flow cytometer (Beckman Coulter) and CytExpert software.

IFN-γ ELISpot. Influenza viral M1 peptide-specific T cell responses were detected by an IFN-γ ELISpot assay (Mabtech, 3321-4AST-2), according to the manufacturer's instructions. In brief, pre-coated 96-well plates with anti-mouse IFN-γ antibody were washed four times with sterile PBS and incubated with RPMI 1640 medium (Gibco) supplemented with 10% FBS for at least 30 minutes at room temperature. Single-cell suspensions were prepared from lung tissues and added to the plate (5×10^5 cells per well). Then, M1 peptide was added to the wells with a final concentration of 5 µg ml^{-1}. After 24–30 hours of incubation in a 37 °C humidified incubator with 5% CO_2, the cells were removed, and the plates were washed five times with PBS. Then, the plates were processed in turn with biotinylated detection antibody R4-6A2, streptavidin-ALP and BCIP/NBT-plus substrate. When distinct spots emerged, the color development was stopped by extensive wash with deionized water. The numbers of the spots were recorded by an ELISpot reader (Cellular Technology).

The following M1 peptides (synthesized by GenScript) were used in this experiment:

$M1_{128–135}$: MGLIYNRM
$M1_{58–66}$: GILGFVFTL

Quantification of M1 antigen presentation. To quantify M1 antigen presentation, Raw264.7 cells at 8×10^5 cells per well were seeded into six-well plates in DMEM supplemented with 10% FBS. Twenty-four hours later, the cells were infected with M1-PTD or M1KO viruses (MOI = 0.1) in DMEM supplemented with 1% FBS and 2 µg ml^{-1} of TPCK-trypsin. The uninfected cells were used as control. Twenty-four hours after infection, the cells were harvested, and the M1 antigen peptides on cell surface were stained with anti-M1 antibody (Sino Biological, 40010-RP01) or customized specific antibody against M1 peptide ($M1_{128–135}$: MGLIYNRM). Samples were analyzed with a FACS flow cytometer (Beckman Coulter) and CytExpert software.

Protein structure prediction. The structure models of PTD-tagged influenza viral proteins were predicted by I-TASSER[32], a composite protein structure prediction approach combining template-based modeling and ab initio loop reconstruction. In brief, the full-length query sequence (influenza viral protein plus the PTD peptide) was searched through the Protein Data Bank by LOMETS[51] for potential templates to model the PTD peptide. Meanwhile, each native structure of influenza viral proteins was specified as an additional structure template by the '-restraint2' flag of the I-TASSER suite. The structure fragments from the templates were assembled into full-length structure by I-TASSER using replica exchange Monte Carlo (REMC) simulation. To ensure that the I-TASSER structure model did not deviate from the native structure of viral protein, the REMC simulation was guided by a generic I-TASSER force field with additional distance restraint to the native structure of viral protein. Conformations from REMC simulation trajectory are clustered by pairwise structure similarity and refined at the atomic level to derive the final model. Apart from the assignment of the influenza viral protein structure for additional template restraint, I-TASSER was run with default parameters. The viral protein portions of all predicted protein structures are almost same to the native structure of influenza viral proteins (template modeling (TM) score >0.9)[52].

Statistical analysis. All experiments were repeated at least two times. Data are presented as mean values ± s.d. Graphing and statistical comparison of the data were performed using GraphPad Prism 8.0 and Microsoft Excel. Two-group comparisons were assessed using the two-tailed Student's *t*-test; comparisons of three or more groups were analyzed by one-way ANOVA with Tukey's or Dunnett's multiple comparisons test. *P* values less than 0.05 were considered statistically significant; exact *P* values are labeled in each figure. Images represent as least two independent experiments for images shown in Figs. 1c and 2b–e,g,h and Extended Data Figs. 2a–c and 6.

Reporting summary. Further information on research design is available in the Nature Research Reporting Summary linked to this article.

Data availability

The gene sequences of WSN influenza virus strain used in this study have been deposited in GenBank under accession numbers CY034138.1, CY034139.1, CY034135.1, CY034134.1, X17336.1, HE802059.1, L25818.1 and CY034136.1. The gene sequences of PR8 influenza virus strain used in this study have been deposited in GenBank under accession numbers CY147541.1, CY147540.1, CY147539.1, CY147534.1, CY147537.1, CY147536.1, CY147535.1 and CY147538.1. 3D structures of M1, PB2, PB1, PA, NP and NS1 have been deposited in the Protein Data Bank (PDB) with PDB IDs: 7JM3, 4WSB, 4WSB, 4IUJ, 2IQH and 4OPH, respectively. Data of VHL expression in human tissues are from GTEx Analysis Release V8 (dbGaP accession number phs000424.v8.p2) (https://gtexportal.org/home/gene/VHL) and also available in the Source Data files. Data of VHL expression in mouse tissues are from RNA sequencing data of E-MTAB-2801 in Expression Atlas and also available in the Source Data files. Data of VHL expression in human lung are from the Human Protein Atlas (http://www.proteinatlas.org/ENSG00000134086-VHL/single+cell+type/lung). All data are available in the manuscript and in Supplementary and Source Data files. No restriction on data availability. Source data are provided with this paper.

References

42. Perez Rubio, A. & Eiros, J. M. Cell culture-derived flu vaccine: present and future. *Hum. Vaccin. Immunother.* **14**, 1874–1882 (2018).
43. Takada, A., Matsushita, S., Ninomiya, A., Kawaoka, Y. & Kida, H. Intranasal immunization with formalin-inactivated virus vaccine induces a broad spectrum of heterosubtypic immunity against influenza A virus infection in mice. *Vaccine* **21**, 3212–3218 (2003).
44. Haredy, A. M. et al. An MDCK cell culture-derived formalin-inactivated influenza virus whole-virion vaccine from an influenza virus library confers cross-protective immunity by intranasal administration in mice. *Clin. Vaccine Immunol.* **20**, 998–1007 (2013).
45. Watanabe, S., Watanabe, T. & Kawaoka, Y. Influenza A virus lacking M2 protein as a live attenuated vaccine. *J Virol* **83**, 5947–5950 (2009).
46. Neumann, G. et al. Generation of influenza A viruses entirely from cloned cDNAs. *Proc. Natl Acad. Sci. USA* **96**, 9345–9350 (1999).
47. Hoffmann, E., Krauss, S., Perez, D., Webby, R. & Webster, R. G. Eight-plasmid system for rapid generation of influenza virus vaccines. *Vaccine* **20**, 3165–3170 (2002).
48. Anchisi, S., Goncalves, A. R., Mazel-Sanchez, B., Cordey, S. & Schmolke, M. Influenza A virus genetic tools: from clinical sample to molecular clone. *Methods Mol. Biol.* **1836**, 33–58 (2018).
49. Lei, C., Yang, J., Hu, J. & Sun, X. On the calculation of $TCID_{50}$ for quantitation of virus infectivity. *Virol. Sin.* **36**, 141–144 (2021).
50. Knudson, D. L. & Tinsley, T. W. Replication of a nuclear polyhedrosis virus in a continuous cell culture of Spodoptera frugiperda: purification, assay of infectivity, and growth characteristics of the virus. *J. Virol.* **14**, 934–944 (1974).
51. Zheng, W. et al. LOMETS2: improved meta-threading server for fold-recognition and structure-based function annotation for distant-homology proteins. *Nucleic Acids Res.* **47**, W429–W436 (2019).
52. Zhang, Y. & Skolnick, J. Scoring function for automated assessment of protein structure template quality. *Proteins* **57**, 702–710 (2004).
53. Karlsson, M. et al. A single-cell type transcriptomics map of human tissues. *Sci. Adv.* **7**, eabh2169 (2021).
54. Noda, T. et al. Architecture of ribonucleoprotein complexes in influenza A virus particles. *Nature* **439**, 490–492 (2006).

Acknowledgements

We acknowledge the Animal Experimental Management Center, Public Technology Service Platform, Shenzhen Institute of Advanced Technology, Chinese Academy of Sciences, for assistance with animal experiments. We acknowledge YuBiolab Ltd., Sinovac Biotech Ltd., TsingKe Biotech Ltd., Genewiz lnc., Corregene Biotech Ltd. and Servicebio Ltd. for technical assistance with animal experiments, gene sequencing, plasmid construction, establishment of cell lines and immunohistochemistry experiments. We thank C. Liu, X. Zhang, S. Huang, Y. Ma, B. Zhang and relevant staffs from the Shenzhen Institute of Synthetic Biology, Shenzhen Institute of Advanced Technology, Chinese Academy of Sciences, for support of technical and experimental platforms. We thank L. Zhu from the Lung Cancer Center, West China Hospital of Sichuan University, for providing paraffin-embedded and frozen sections of human lung tissue. We acknowledge the Genotype-Tissue Expression (GTEx) Project and/or Portal supported by the Common Fund of the Office of the Director of the National Institutes of Health and by NCI, NHGRI, NHLBI, NIDA, NIMH and NINDS. This work was supported by the National Natural Science Foundation of China (grant to L.S., grant no. 11932014 to X.L., and grant no. 81802456 to H.T.), the China-U.S. Collaborative Program on Emerging and Re-emerging Infectious Diseases (grant no. E2900901-02 to W.T.), Guangdong Basic and Applied Basic Research Foundation (grant no. 2019A1515110615 to H.L.), Natural Science Foundation Program of Shaanxi Province of China (grant no. 2020JQ-545 to H.T.), the Key R&D Program of Shanxi Province of China (grant to W.T.), China Postdoctoral Science Foundation (grant no. 2019TQ0206 to H.L.), and the Shenzhen Institute of Synthetic Biology, Shenzhen Institute of Advanced Technology, Chinese Academy of Sciences (grant to L.S.).

Author contributions

L.S. conceived this study and designed the experiments. L.S., Q.S. and J.L. performed and analyzed experiments, with other authors assisting with experiments and data analysis. L.S. wrote the manuscript, with all authors providing feedback.

Competing interests

L.S., Q.S., J.L., L.C., J.S. and X.X. are inventors on the relevant patent applications held by the Shenzhen Institute of Advanced Technology, Chinese Academy of Sciences. The remaining authors declare no competing financial interests.

Additional information

Extended data is available for this paper at https://doi.org/10.1038/s41587-022-01381-4.

Supplementary information The online version contains supplementary material available at https://doi.org/10.1038/s41587-022-01381-4.

Correspondence and requests for materials should be addressed to Longlong Si.

Peer review information *Nature Biotechnology* thanks the anonymous reviewers for their contribution to the peer review of this work.

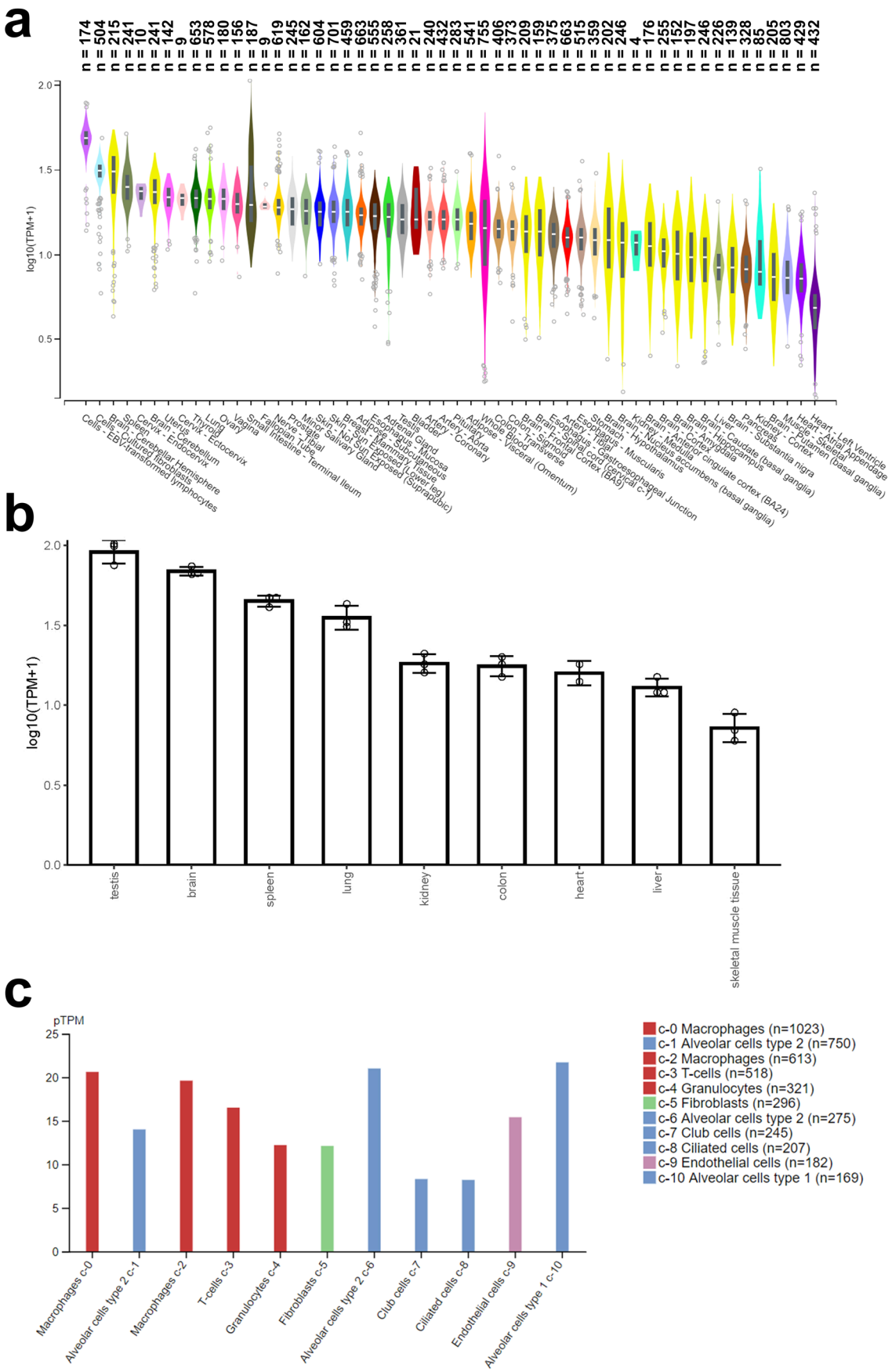

Extended Data Fig. 1 | See next page for caption.

Extended Data Fig. 1 | VHL is widely expressed in tissues of human and mouse. a, Expression of VHL in human tissues. Data are from GTEx Analysis Release V8 (dbGaP accession number phs000424.v8.p2) (https://gtexportal.org/home/gene/VHL). Box plots are shown as median and 25th and 75th percentiles; points are displayed as outliers if they are above or below 1.5 times the interquartile range. TPM, transcripts per million. **b**, Expression of VHL in mouse tissues based on RNA-seq data of E-MTAB-2801 in Expression Atlas. Data are presented as mean ± SD; n = 2 for heart and 3 for others. **c**, Expression of VHL in the human lung. Data are from the Human Protein Atlas (http://www.proteinatlas.org/ENSG00000134086-VHL/single+cell+type/lung)[53]. pTPM, transcripts per million protein coding genes.

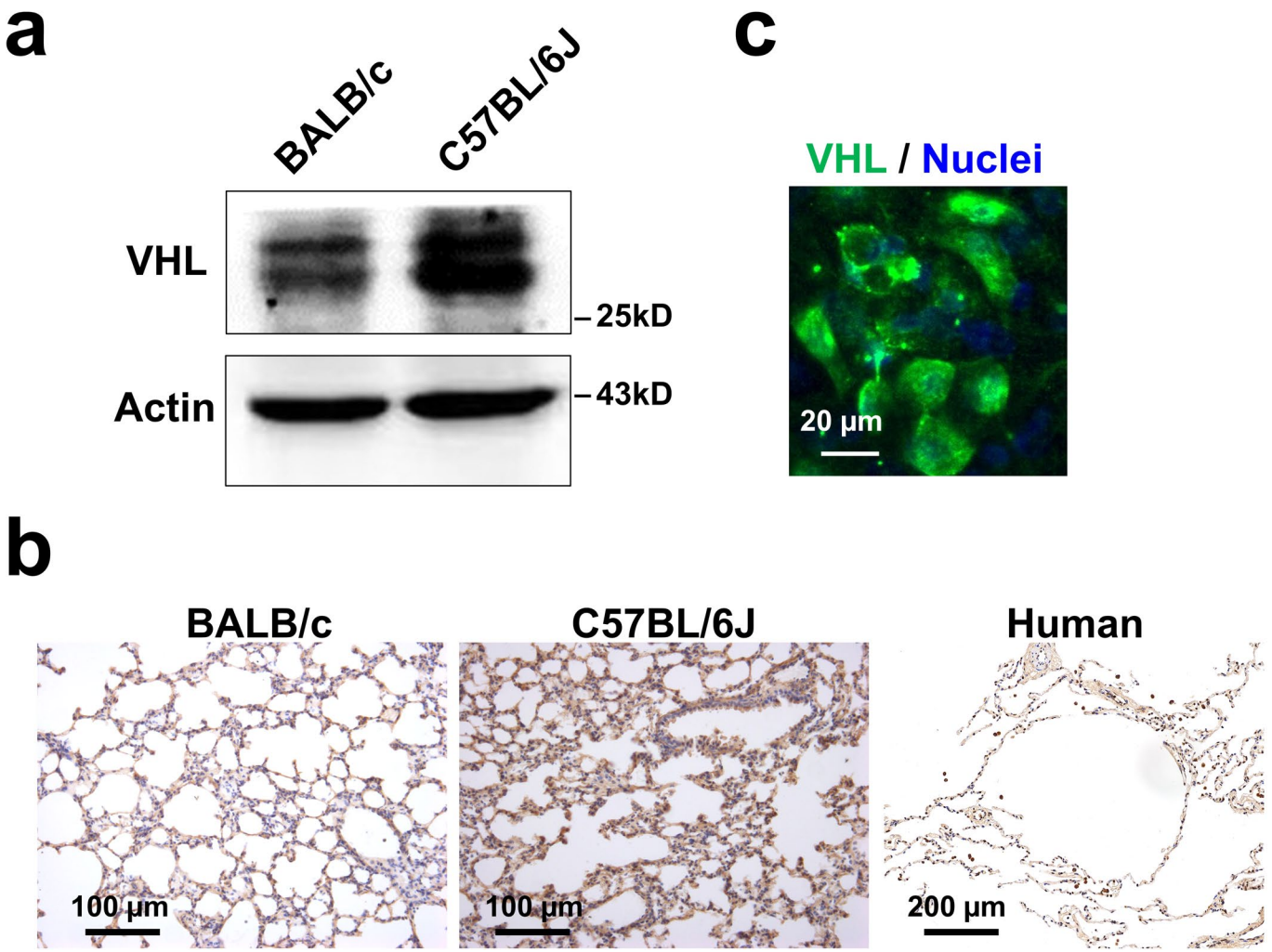

Extended Data Fig. 2 | VHL is widely expressed in lungs of mouse and human. a, Western blotting images showing the expression of VHL in lungs of BALB/c and C57BL/6 J mice. **b**, Immunohistochemistry images showing the expression of VHL (brown) in lungs of BALB/c mouse, C57BL/6 J mouse, and human (n = 3). **c**, Immunofluorescence image showing the expression of VHL in primary human lung alveolar epithelium cultured on Transwells. Green, VHL; blue, nuclei. All experiments were repeated at least two times.

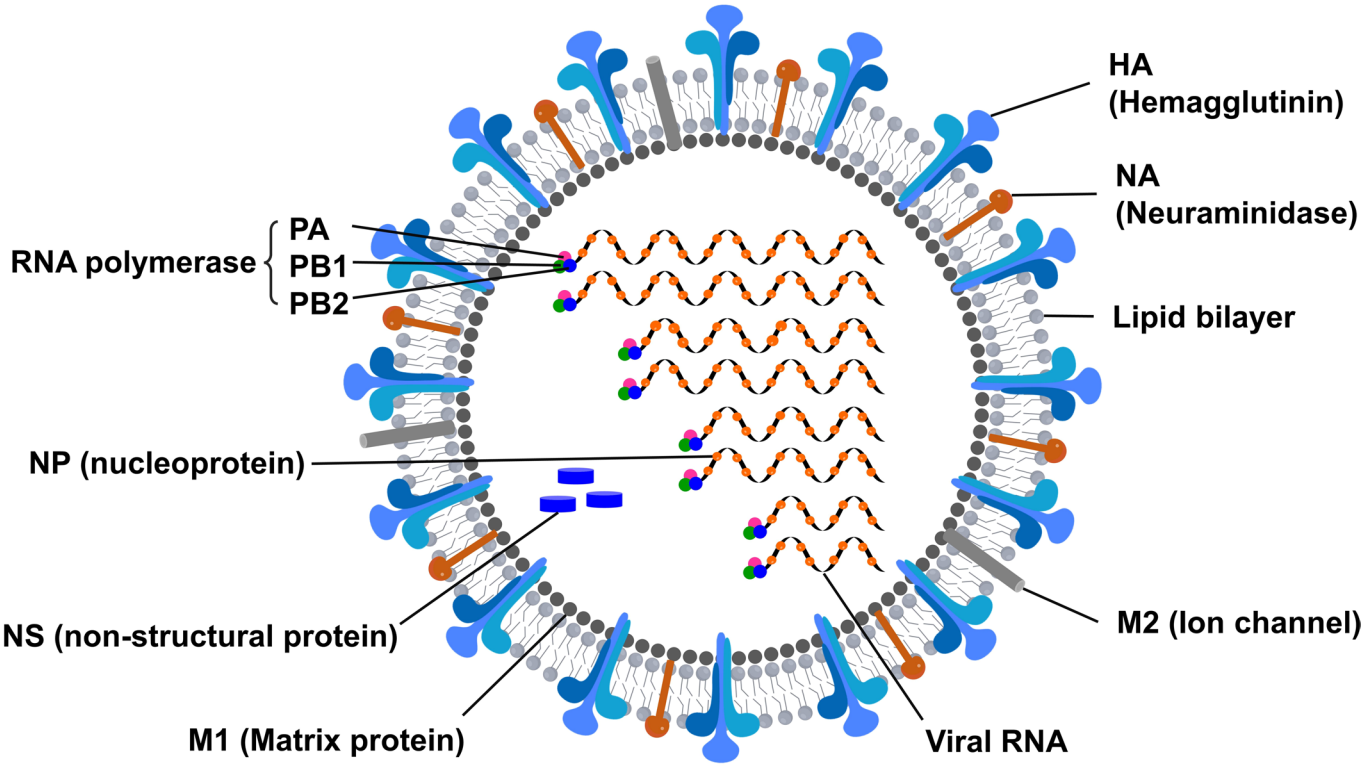

Extended Data Fig. 3 | Schematic structure model of the influenza A virion. Influenza A virions are enveloped spherical structures with diameters of 80–120 nm[54]. The genome of each influenza A virion contains eight single-stranded negative-sense RNA segments, encoding 10 main viral proteins: hemagglutinin (HA), neuraminidase (NA), matrix protein 1 (M1), M2, polymerase basic protein 1 (PB1), polymerase basic protein 2 (PB2), polymerase acidic protein (PA), nucleoprotein (NP), nonstructural protein 1 (NS1), and nuclear export protein (NEP, also known as NS2). HA and NA are two main antigenic determinants of influenza virus, which are on the surface of the viral envelope and mediate viral entry into host cells and release of progeny virions from host cells, respectively. M2 is the third integral membrane protein, which forms ion channels in virion particles and has roles in viral entry, assembly, and budding. M1, the most abundant protein in the virion, lines the internal surface of the viral lipid bilayer and mediates the interactions between the viral membrane and ribonucleoprotein (RNP). The RNP is a complex structure composed of multiple copies of the viral NP, which wraps eight viral RNA genome segments, and a single RNA polymerase, which binds to the termini of each RNA genome segment. The RNA polymerase has three subunits: PB1, PB2, and PA, which are responsible for viral replication and transcription[17,54]. NS1 plays an important role in evasion of the host innate immune system and facilitates viral replication. NEP mediates the export of the newly synthesized viral RNP from the nucleus into the cytoplasm.

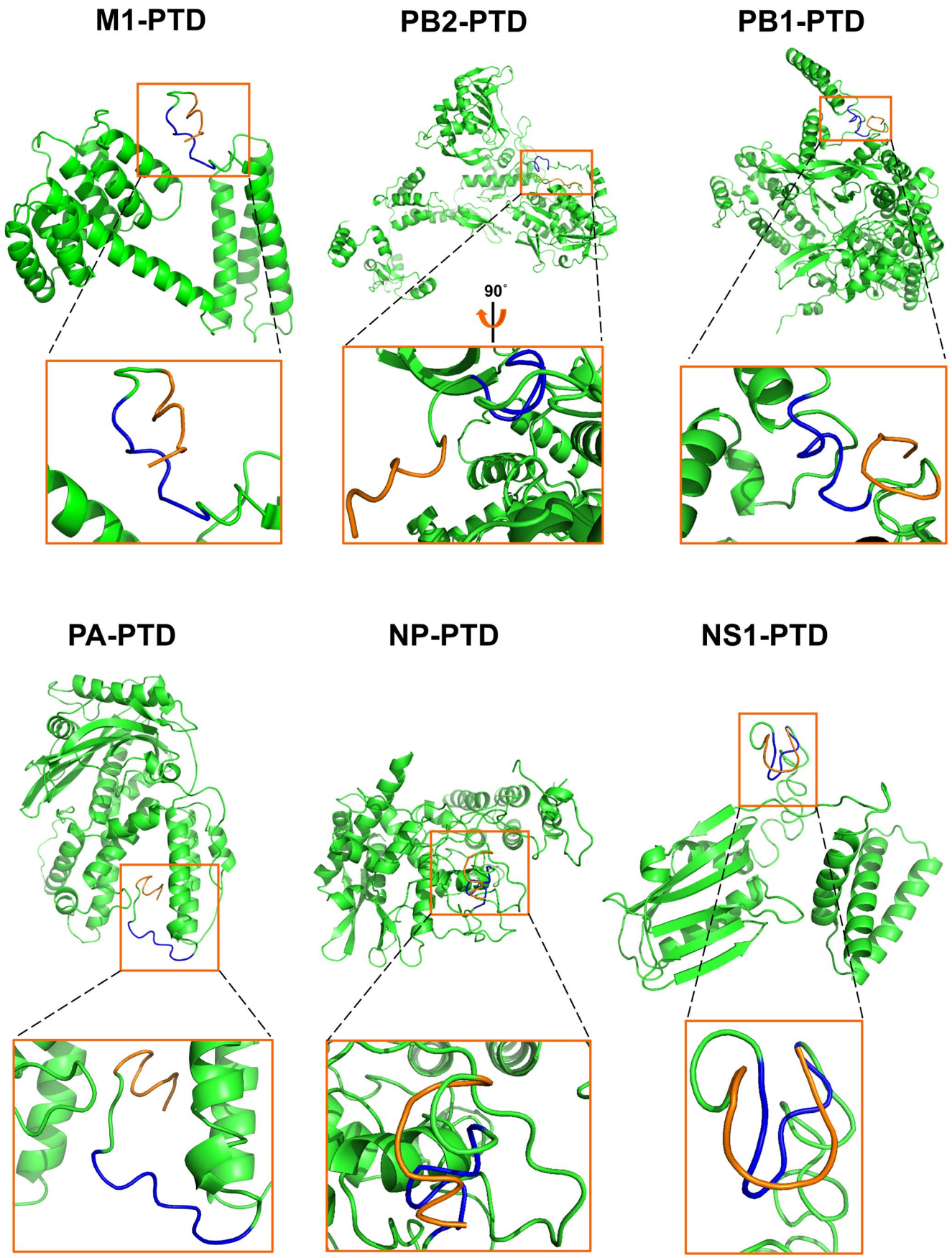

Extended Data Fig. 4 | See next page for caption.

Extended Data Fig. 4 | Structure prediction of PTD-tagged influenza viral proteins according to I-TASSER[32]. Green, viral protein; blue, TEVcs linker; orange, proteasome-targeting peptides. Top images showing the overall structures of influenza viral proteins containing PTD, bottom images showing the close-up views on PTD domain in each influenza viral protein. The PDB IDs of M1, PB2, PB1, PA, NP, and NS1 are 7JM3, 4WSB, 4WSB, 4IUJ, 2IQH, and 4OPH, respectively.

```
Template      1 agcaaaagcaggtagatattgaaagatgagtcttctaaccgaggtcgaaacgtacgttctctctatcgtcccgtcaggccccctcaaagccgagatcgca    100
                ||||||||||||||||||||||||||||||||||||||||||||||||||||||||||||||||||||||||||||||||||||||||||||||||||||
M1-PTD        1 agcaaaagcaggtagatattgaaagatgagtcttctaaCCGAGGTCGAAACGTACGTTCTCTCTATCGTCCCGTCAGGCCCCCTCAAAGCCGAGATCGCA    100

Template    101 cagagacttgaagatgtctttgcagggaagaacaccgatcttgaggttctcatggaatggctaaagacaagaccaatcctgtcacctctgactaagggga    200
                ||||||||||||||||||||||||||||||||||||||||||||||||||||||||||||||||||||||||||||||||||||||||||||||||||||
M1-PTD      101 CAGAGACTTGAAGATGTCTTTGCAGGGAAGAACACCGATCTTGAGGTTCTCATGGAATGGCTAAAGACAAGACCAATCCTGTCACCTCTGACTAAGGGGA    200

Template    201 ttttaggatttgtgttcacgctcaccgtgcccagtgagcggggactgcagcgtagacgctttgtccaaaatgctcttaatgggaacggagatccaaataa    300
                ||||||||||||||||||||||||||||||||||||||||||||||||||||||||||||||||||||||||||||||||||||||||||||||||||||
M1-PTD      201 TTTTAGGATTTGTGTTCACGCTCACCGTGCCCAGTGAGCGGGGACTGCAGCGTAGACGCTTTGTCCAAAATGCTCTTAATGGGAACGGAGATCCAAATAA    300

Template    301 catggacaaagcagttaaactgtataggaagcttaagagggagataacattccatggggccaaagaaatagcactcagttattctgctggtgcacttgcc    400
                ||||||||||||||||||||||||||||||||||||||||||||||||||||||||||||||||||||||||||||||||||||||||||||||||||||
M1-PTD      301 CATGGACAAAGCAGTTAAACTGTATAGGAAGCTTAAGAGGGAGATAACATTCCATGGGGCCAAAGAAATAGCACTCAGTTATTCTGCTGGTGCACTTGCC    400

Template    401 agttgtatgggcctcatatacaacaggatgggggctgtgaccactgaagtggcatttggcctggtatgcgcaacctgtgaacagattgctgactcccagc    500
                ||||||||||||||||||||||||||||||||||||||||||||||||||||||||||||||||||||||||||||||||||||||||||||||||||||
M1-PTD      401 AGTTGTATGGGCCTCATATACAACAGGATGGGGGCTGTGACCACTGAAGTGGCATTTGGCCTGGTATGCGCAACCTGTGAACAGATTGCTGACTCCCAGC    500

Template    501 atcggtctcataggcaaatggtgacaacaaccaatccactaatcagacatgagaacagaatggttctagccagcactacagctaaggctatggagcaaat    600
                ||||||||||||||||||||||||||||||||||||||||||||||||||||||||||||||||||||||||||||||||||||||||||||||||||||
M1-PTD      501 ATCGGTCTCATAGGCAAATGGTGACAACAACCAATCCACTAATCAGACATGAGAACAGAATGGTTCTAGCCAGCACTACAGCTAAGGCTATGGAGCAAAT    600

Template    601 ggctggatcgagtgagcaagcagcagaggccatggatattgctagtcaggccaggcaaatggtgcaggcgatgagaaccgttgggactcatcctagctcc    700
                ||||||||||||||||||||||||||||||||||||||||||||||||||||||||||||||||||||||||||||||||||||||||||||||||||||
M1-PTD      601 GGCTGGATCGAGTGAGCAAGCAGCAGAGGCCATGGATATTGCTAGTCAGGCCAGGCAAATGGTGCAGGCGATGAGAACCGTTGGGACTCATCCTAGCTCC    700

Template    701 agtgctggtctaaaagatgatcttcttgaaaatttgcaggcctatcagaaacgaatgggggtgcagatgcaacgattcaaggttctggtggtgagaatc    781
                ||||||||||||||||||||||||||||||||||||||||||||||||||||||||||||||||||||||||||||||||||||||||||||||||||||
M1-PTD      701 AGTGCTGGTCTAAAAGATGATCTTCTTGAAAATTTGCAGGCCTATCAGAAACGAATGGGGGTGCAGATGCAACGATTCAACGGTTCTGGTGGTGAGAATC    800

Template    782 tgtacttccaaggtggatctggagcattggccccctacattccatgatcctctcgtcattgcagcaaatatcattggaatcttgcacttgatattgtgga    837
                ||||||||||||||||||||||||||||||||||||||||||||||||||||||||||||||||||||||||||||||||||||||||||||||||||||
M1-PTD      801 TGTACTTCCAAGGTGGATCTGGAGCATTGGCCCCCTACATTCCATGATCCTCTCGTCATTGCAGCAAATATCATTGGAATCTTGCACTTGATATTGTGGA    900

Template    838 ttcttgatcgtctttttttcaaatgcatttatcgtcgctttaaatacggtttgaaaagagggccttctacggaaggagtgccagagtctatgagggaaga    937
                ||||||||||||||||||||||||||||||||||||||||||||||||||||||||||||||||||||||||||||||||||||||||||||||||||||
M1-PTD      901 TTCTTGATCGTCTTTTTTTCAAATGCATTTATCGTCGCTTTAAATACGGTTTGAAAAGAGGGCCTTCTACGGAAGGAGTGCCAGAGTCTATGAGGGAAGA   1000

Template    938 atatcgaaaggaacagcagaatgctgtggatgttgacgatggtcattttgtcaacatagagctggagtaa   1007
                ||||||||||||||||||||||||||||||||||||||||||||||||||||||||||||||||||||||
M1-PTD     1001 ATATCGAAAGGAACAGCAGAATGCTGTGGATGTTGACGATGGTCATTTTGTCAACATAgagctggagtaa   1070
```

PTD

Extended Data Fig. 5 | Verification of the genetic stability of M1-PTD by sequencing after 20 passages in MDCK-TEVp cells. The gene sequence used to construct the M1-PTD was used as the template.

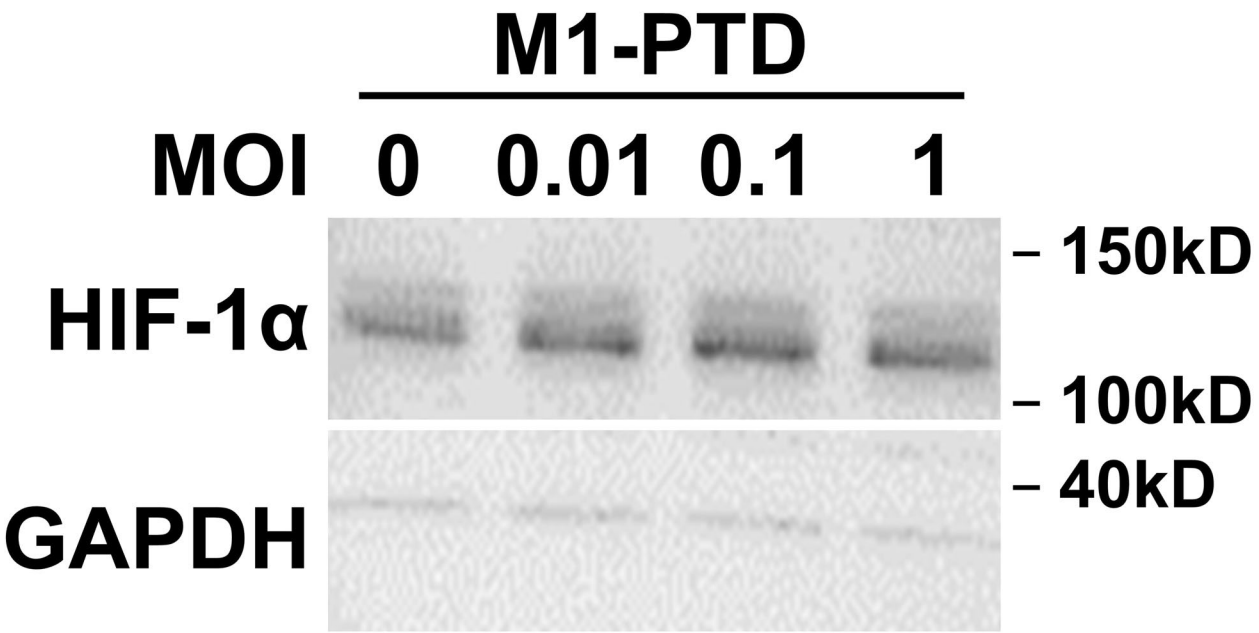

Extended Data Fig. 6 | M1-PTD infection had no effect on HIF-1α, the endogenous substrate of VHL, even at MOI = 1.0. MDCK.2 cells were infected with M1-PTD (MOI = 0, 0.01, 0.1, or 1.0) and analyzed for HIF-1α protein levels by western blotting at 48 h post-infection. The experiment was repeated two times.

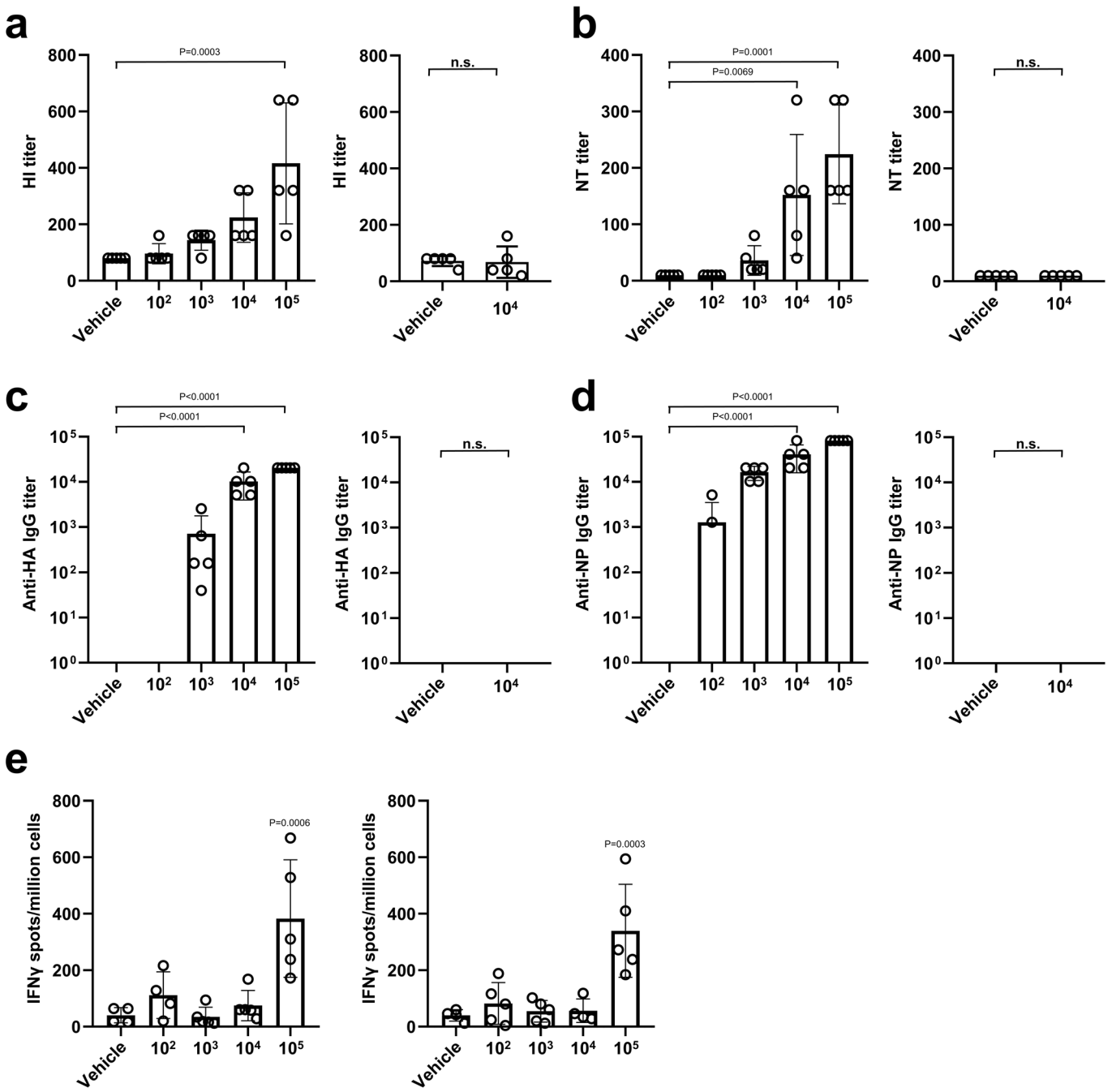

Extended Data Fig. 7 | The dose-dependent immune responses elicited by M1-PTD in WT mice and the immune responses elicited by M1-PTD in BALB/c Nude mice. a, HI antibody responses elicited by indicated dosages of M1-PTD in the sera of WT BALB/c (left) and BALB/c Nude (right) mice at day 21 post-vaccination (n = 5). Data are plotted for individual mice and overlaid with mean ± SD; left graph, one-way ANOVA with Dunnett's multiple comparisons test; right graph, unpaired two-tailed t-test; n.s., not significant. **b**, NT antibody responses elicited by indicated dosages of M1-PTD in the sera of WT BALB/c (left) and BALB/c Nude (right) mice at day 21 post-vaccination (n = 5). Data are plotted for individual mice and overlaid with mean ± SD; left graph, one-way ANOVA with Dunnett's multiple comparisons test; right graph, unpaired two-tailed t-test; n.s., not significant. **c**, Anti-HA antibody responses elicited by indicated dosages of M1-PTD in the sera of WT BALB/c (left) and BALB/c Nude (right) mice at day 21 post-vaccination (n = 5). Data are plotted for individual mice and overlaid with mean ± SD; left graph, one-way ANOVA with Dunnett's multiple comparisons test; right graph, unpaired two-tailed t-test; n.s., not significant. **d**, Anti-NP antibody responses elicited by indicated dosages of M1-PTD in the sera of WT BALB/c (left) and BALB/c Nude (right) mice at day 21 post-vaccination (n = 5). Data are plotted for individual mice and overlaid with mean ± SD; left graph, one-way ANOVA with Dunnett's multiple comparisons test; right graph, unpaired two-tailed t-test; n.s., not significant. Note that M1-PTD did not induce immune response in T cell-deficient BALB/c Nude mice, indicating that T cell response may be the driver for the immunity elicited by M1-PTD. **e**, Viral M1 antigen-specific T cell responses elicited by indicated dosages of M1-PTD in the lungs of WT C57BL/6 J mice at day 7 post-vaccination (n = 5), measured by ELISpot assay. Two peptides, $M1_{128-135}$ MGLIYNRM (left) and $M1_{58-66}$ GILGFVFTL (right), were used as the stimuli. IFNγ-expressing cells per million cells were shown. Data are plotted for individual mice and overlaid with mean ± SD; one-way ANOVA with Dunnett's multiple comparisons test.

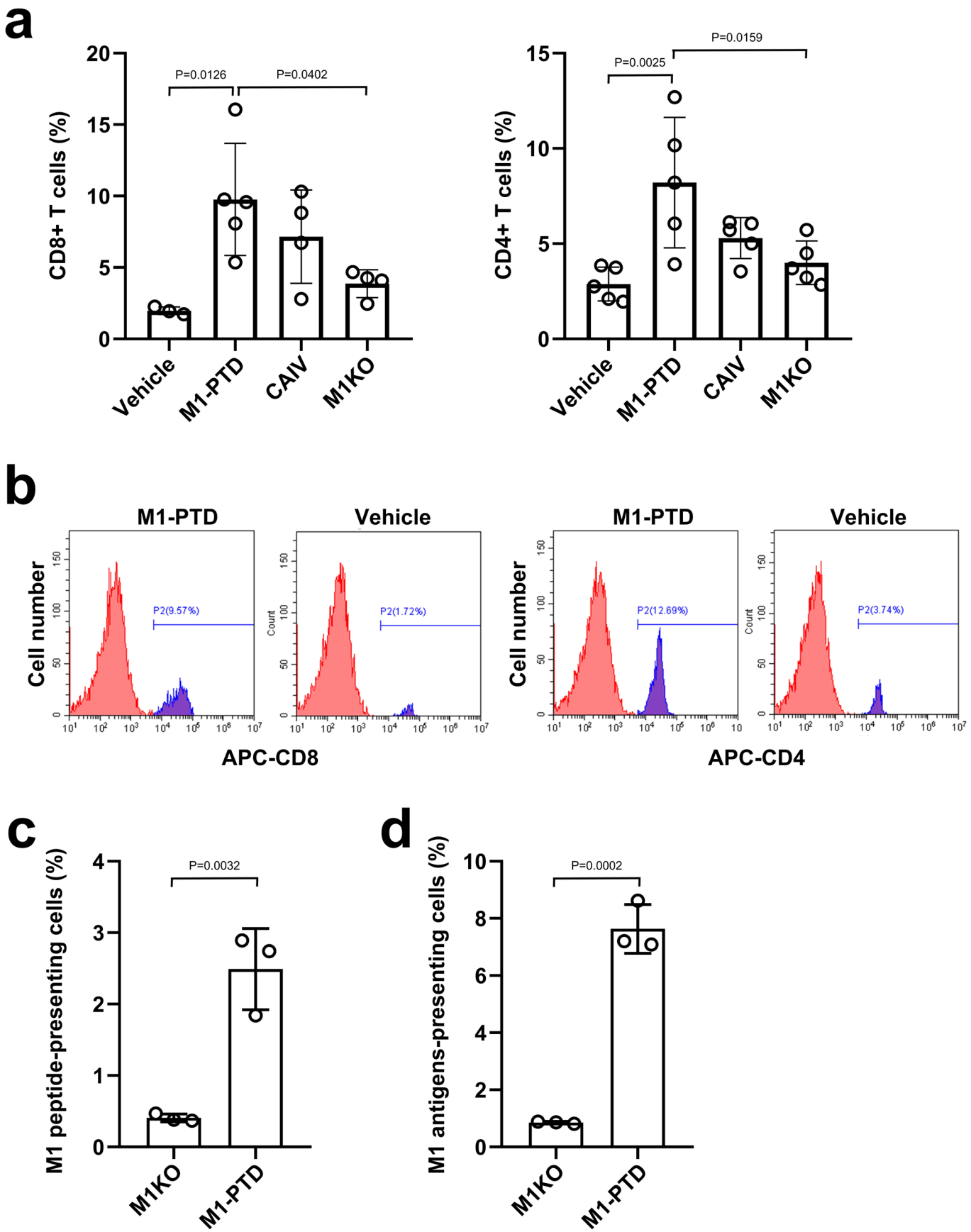

Extended Data Fig. 8 | See next page for caption.

Extended Data Fig. 8 | T cell responses induced by M1-PTD and M1 antigen presentation mediated by PTD. a, CD8 and CD4 T cell responses elicited by 10^5 PFU of M1-PTD, CAIV, and M1-KO vaccines in lungs of C57BL/6 J mice at day 7 post-vaccination, measured by flow cytometry. Data are plotted for individual mice and overlaid with mean ± SD; n = 3 mice for Vehicle in left graph, 4 mice for CAIV in left graph, and 5 mice for all other groups; one-way ANOVA with Tukey's multiple comparisons test. **b**, Representative flow cytometry histograms are shown for lung samples from mice vaccinated with 10^5 PFU of M1-PTD. Purple, stained cells; red, unstained cells. **c and d**, PTD-mediated M1 degradation increases M1 antigen presentation in Raw264.7 cells. Raw264.7 cells were infected with M1-PTD or M1KO virus (MOI = 0.1). 24 hours after infection, M1 antigen presentation on the surface of Raw264.7 cells was detected by an anti-M1 peptide ($M1_{128\text{-}135}$: MGLIYNRM) antibody (**c**) or an anti-M1 antibody (**d**) using flow cytometry. Data are presented as mean ± SD; n = 3 biological replicates; unpaired two-tailed t-test.

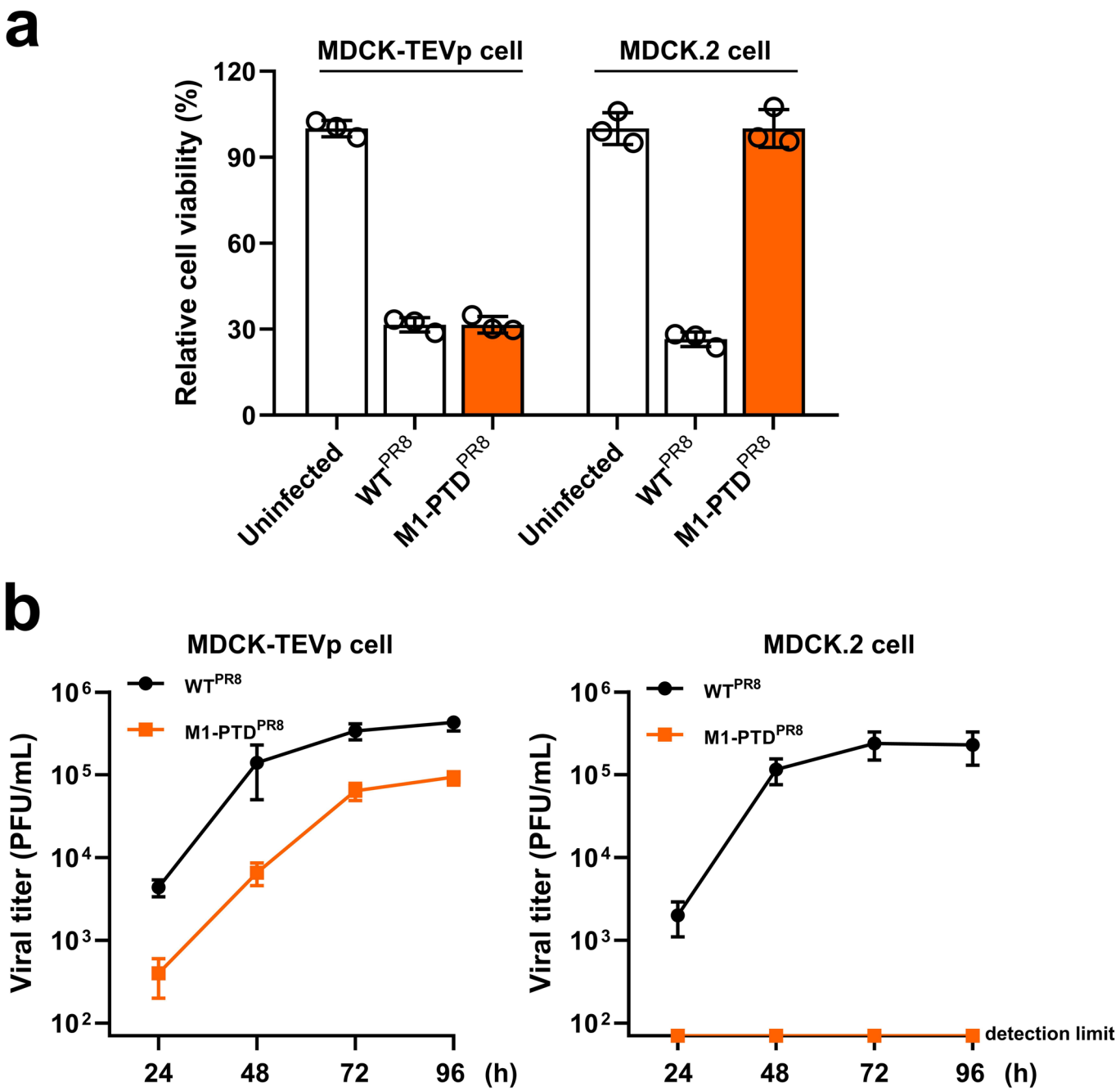

Extended Data Fig. 9 | Characterization of the broad applicability of PROTAC virus vaccine strategy. a, Generation and characterization of PROTAC virus M1-PTD^{PR8} by incorporating PTD to M1 protein of influenza A/Puerto Rico/8/1934 (H1N1) virus (PR8). Characterization of the efficient propagation of M1-PTD^{PR8} in MDCK-TEVp cells and not in conventional MDCK.2 cells by CPE measured by CellTiter-Glo assay. Data are presented as mean ± SD; n = 3 biological replicates. **b**, Multicycle replication kinetics curves of M1-PTD^{PR8} in MDCK-TEVp and conventional MDCK.2 cells. The detection limit is 70 PFU/mL. Data are presented as mean ± SD; n = 3 biological replicates.

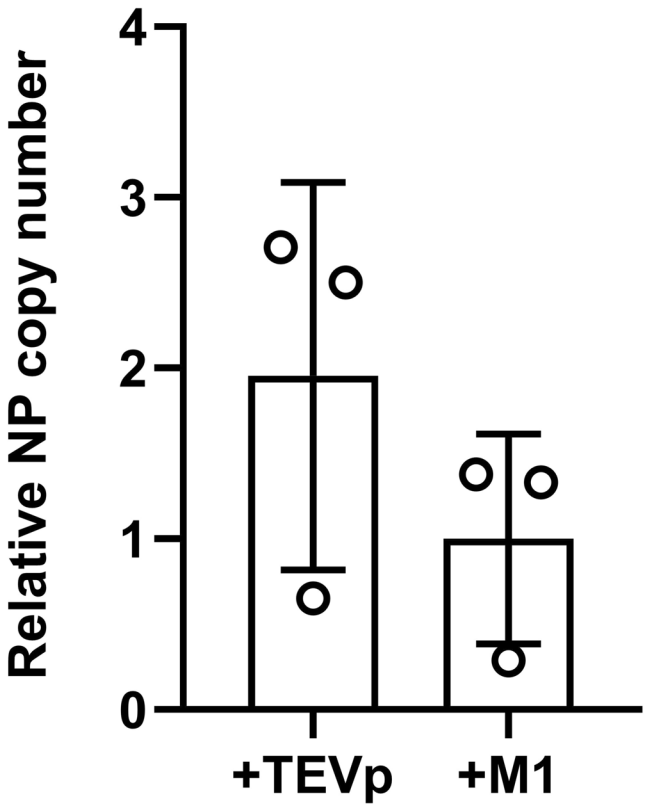

Extended Data Fig. 10 | Replication of M1-PTD in TEVp- or viral M1-expressing HEK293T cells. Relative copy numbers of NP gene of M1-PTD viruses in viral supernatants after 2 days of propagation in TEVp-expressing or viral M1-expressing HEK293T cells indicate that M1-PTD can efficiently replicate in both types of cells. Data are presented as mean ± SD; n = 3 biological replicates.

nature research

Corresponding author(s): Longlong Si

Last updated by author(s): May 25, 2022

Reporting Summary

Nature Research wishes to improve the reproducibility of the work that we publish. This form provides structure for consistency and transparency in reporting. For further information on Nature Research policies, see Authors & Referees and the Editorial Policy Checklist.

Statistics

For all statistical analyses, confirm that the following items are present in the figure legend, table legend, main text, or Methods section.

n/a	Confirmed	
☐	☒	The exact sample size (*n*) for each experimental group/condition, given as a discrete number and unit of measurement
☐	☒	A statement on whether measurements were taken from distinct samples or whether the same sample was measured repeatedly
☐	☒	The statistical test(s) used AND whether they are one- or two-sided *Only common tests should be described solely by name; describe more complex techniques in the Methods section.*
☒	☐	A description of all covariates tested
☒	☐	A description of any assumptions or corrections, such as tests of normality and adjustment for multiple comparisons
☐	☒	A full description of the statistical parameters including central tendency (e.g. means) or other basic estimates (e.g. regression coefficient) AND variation (e.g. standard deviation) or associated estimates of uncertainty (e.g. confidence intervals)
☐	☒	For null hypothesis testing, the test statistic (e.g. *F*, *t*, *r*) with confidence intervals, effect sizes, degrees of freedom and *P* value noted *Give P values as exact values whenever suitable.*
☒	☐	For Bayesian analysis, information on the choice of priors and Markov chain Monte Carlo settings
☒	☐	For hierarchical and complex designs, identification of the appropriate level for tests and full reporting of outcomes
☒	☐	Estimates of effect sizes (e.g. Cohen's *d*, Pearson's *r*), indicating how they were calculated

Our web collection on statistics for biologists contains articles on many of the points above.

Software and code

Policy information about availability of computer code

Data collection	Images were taken with the built-in software of fluorescence microscope (NIKON ECLIPSE Ti2-E, Japan). Image processing was done using NIS-Elements (NIKON , Japan). I-TASSER v5.1 and LOMETS (version 3) was used for the protein structure prediction. Beckman Coulter CytoFlex S was used for cell sorting. CytExpert Version 2.4.1 software was used for cell sorting.
Data analysis	Graphpad Prism 8.0, Microsoft Excel v16, CytExpert Version 2.4.1 software

For manuscripts utilizing custom algorithms or software that are central to the research but not yet described in published literature, software must be made available to editors/reviewers. We strongly encourage code deposition in a community repository (e.g. GitHub). See the Nature Research guidelines for submitting code & software for further information.

Data

Policy information about availability of data

All manuscripts must include a data availability statement. This statement should provide the following information, where applicable:

- Accession codes, unique identifiers, or web links for publicly available datasets
- A list of figures that have associated raw data
- A description of any restrictions on data availability

The gene sequences of WSN influenza virus strain used in this study have been deposited in GenBank under accession numbers CY034138.1, CY034139.1, CY034135.1, CY034134.1, X17336.1, HE802059.1, L25818.1, and CY034136.1. The gene sequences of PR8 influenza virus strain used in this study have been deposited in GenBank under accession numbers CY147541.1, CY147540.1, CY147539.1, CY147534.1, CY147537.1, CY147536.1, CY147535.1, and CY147538.1. 3D structures of M1, PB2, PB1, PA, NP, and NS1 have been deposited in Protein Data Bank (PDB) with PDB IDs: 7JM3, 4WSB, 4WSB, 4IUJ, 2IQH, and 4OPH, respectively. Data of VHL expression in human tissues are from GTEx Analysis Realease V8 (dbGaP accession number phs000424.v8.p2) (https://gtexportal.org/home/gene/VHL) and also available in the source data files. Data of VHL expression in mouse tissues are from RNA-seq data of E-MTAB-2801 in Expression Atlas and also available in the source data files. Data of VHL expression in human lung are from the Human Protein Atlas (http://www.proteinatlas.org/ENSG00000134086-VHL/single+cell+type/lung). All data are available in the manuscript, supplementary, and source data files. No restriction on data availability.

Field-specific reporting

Please select the one below that is the best fit for your research. If you are not sure, read the appropriate sections before making your selection.

☒ Life sciences ☐ Behavioural & social sciences ☐ Ecological, evolutionary & environmental sciences

For a reference copy of the document with all sections, see nature.com/documents/nr-reporting-summary-flat.pdf

Life sciences study design

All studies must disclose on these points even when the disclosure is negative.

Sample size	Sample sizes in animal model studies were chosen as guided by the literatures for similar studies, as described in refs. 3-7 and 9-11. All tissue culture experiments were performed with a minimum of three independent biological replicates, which were sufficient to detect significant differences.
Data exclusions	No data were excluded from the analyses.
Replication	Each experiment was repeated independently at least two times. All attempts at replication were successful.
Randomization	All samples were randomly assigned into groups in all studies.
Blinding	Blinding was used for data analysis of animal study - including the samples given to animals for vaccination, and the samples given to animals for viral challenge. Blinding was not required for other experiments presented because the experiments are highly quantitative and controlled.

Reporting for specific materials, systems and methods

We require information from authors about some types of materials, experimental systems and methods used in many studies. Here, indicate whether each material, system or method listed is relevant to your study. If you are not sure if a list item applies to your research, read the appropriate section before selecting a response.

Materials & experimental systems

n/a	Involved in the study
☐	☒ Antibodies
☐	☒ Eukaryotic cell lines
☒	☐ Palaeontology
☐	☒ Animals and other organisms
☐	☒ Human research participants
☒	☐ Clinical data

Methods

n/a	Involved in the study
☒	☐ ChIP-seq
☐	☒ Flow cytometry
☒	☐ MRI-based neuroimaging

Antibodies

Antibodies used	Anti-M1 antibody (40010-RP01, 1:1,000 dilution for western blotting, 1:400 for immunofluorescence staining, 1:100 dilution for flow cytometry) was purchased from Sino Biological. Rabbit anti-M1 peptide (MGLIYNRM) antibody (1:100 dilution for flow cytometry) was custom made by Sino Biological. Anti-M1 antibody (NBP2-14995, 1:1,000 dilution for western blotting, 1:200 dilution for immunofluorescence staining) was purchased from Novus Biologicals. Anti-M1 antibody (ab25918, 1:1,000 dilution for western blotting), anti-NP (ab128193, clone C43, 1:200 dilution for immunofluorescence staining), anti-HIF1α (ab179483, clone EPR16897, 1:500 dilution) and anti-rabbit IgG-HRP (ab6721, 1:2,000 dilution) antibodies were purchased from Abcam. Anti-TEVp antibody (NBP1-97669, 1:500 dilution) was purchased from Novus Biologicals. Anti-TEVp antibody (PAB19931, 1:500 dilution) was purchased from Abnova. Anti-β-tubulin antibody (700608, clone 1E1, 1:10,000 dilution) was purchased from Zen Bio. Anti-VHL antibody (GTX101087, 1:1,000 dilution for western blotting, 1:100 dilution for immunofluorescence staining and immunohistochemistry staining) and anti-GAPDH antibody (GTX100118, 1:5,000 dilution) were purchased from GeneTex. Anti-rabbit IgG-HRP (7074S, 1: 4,000 dilution) was purchased from Cell Signaling Technology. Anti-rabbit IgG-HRP (SA00001-2, 1:2,000 dilution) and anti-mouse IgG-HRP (SA00001-1, 1:2,000 dilution) were purchased from Proteintech. Alexa Fluor 488 goat anti-mouse IgG (A11001, 1:1,000 dilution) and Alexa Fluor 488 goat anti-rabbit IgG (A11034, 1:1,000 dilution for immunofluorescence staining, 1:500 dilution for flow cytometry) were purchased from Life Technologies. APC anti-mouse CD8a antibody (100712, 1:100 dilution) and APC anti-mouse CD4 antibody (100412, 1:125 dilution) were purchased from BioLegend. Anti-mouse CD8a-FITC antibody (553031, 1:100 dilution) was purchased from BD Bioscience. HRP-conjugated anti-mouse IgA antibody (ab97235, 1:2,000 dilution) was purchased from Abcam. HRP-conjugated anti-ferret IgA antibody (618-103-006, 1:2,000 dilution) was purchased from Rockland Immunochemicals.
Validation	Anti-M1 antibody (Sino Biological, 40010-RP01) and Rabbit anti-M1 peptide (MGLIYNRM) were validated in Fig. 2c-e, g and Extended Data Fig. 8c,d. Anti-M1 antibody (NBP2-14995) was validated by the vendor Novus Biologicals. Vendor's website: https://www.novusbio.com/

products/influenza-a-h1n1-m1-antibody_nbp2-14995

Anti-M1 antibody (ab25918) was validated by the vendor Abcam. Vendor's website: https://www.abcam.com/avian-influenza-matrix-protein-i-antibody-ab25918.html

Anti-NP (ab128193, clone C43) was validated by the vendor Abcam. Vendor's website: https://www.abcam.com/influenza-a-virus-nucleoprotein-antibody-c43-ab128193.html

Anti-HIF1α (ab179483, clone EPR16897) was validated by the vendor Abcam. Vendor's website: https://www.abcam.com/hif-1-alpha-antibody-epr16897-ab179483.html

Anti-rabbit IgG-HRP (ab6721) was validated by the vendor Abcam. Vendor's website: https://www.abcam.com/goat-rabbit-igg-hl-hrp-ab6721.html

Anti-TEVp antibody (NBP1-97669) was validated by the vendor Novus Biologicals. https://www.novusbio.com/products/tev-protease-antibody_nbp1-97669

Anti-TEVp antibody (PAB19931) was validated by the vendor Abnova. Vendor's website: http://www.abnova.com/products/products_detail.asp?catalog_id=PAB19931

Anti-β-tubulin antibody (700608, clone 1E1) was validated by the vendor Zen Bio. Vendor's wesbite: http://en.zen-bio.cn/prod_view.aspx?IsActiveTarget=True&TypeId=132&Id=408038&FId=t3:132:3

Anti-VHL antibody (GTX101087) was validated by the vendor GeneTex. Vendor's website: https://www.genetex.cn/Product/Detail/Von-Hippel-Lindau-antibody/GTX101087

Anti-GAPDH antibody (GTX100118, 1:5,000 dilution) was validated by the vendor GeneTex. Vendor's website: https://www.genetex.cn/Product/Detail/GAPDH-antibody/GTX100118

Anti-rabbit IgG-HRP (7074S) was validated by the vendor Cell Signaling Technology. Vendor's website: https://www.cellsignal.com/products/secondary-antibodies/anti-rabbit-igg-hrp-linked-antibody/7074?site-search-type=Products&N=4294956287&Ntt=7074s&fromPage=plp&_requestid=349807

Anti-rabbit IgG-HRP (SA00001-2) was validated by the vendor Proteintech. Vendor's website: https://www.ptglab.com/products/HRP-conjugated-Affinipure-Goat-Anti-Rabbit-IgG-H-L-secondary-antibody.htm

Anti-mouse IgG-HRP (SA00001-1) was validated by the vendor Proteintech. Vendor's website: https://www.ptglab.com/products/HRP-conjugated-Affinipure-Goat-Anti-Mouse-IgG-H-L-secondary-antibody.htm

Alexa Fluor 488 goat anti-mouse IgG (A11001) was validated by the vendor. Vendor website: https://www.thermofisher.cn/cn/zh/antibody/product/Goat-anti-Mouse-IgG-H-L-Cross-Adsorbed-Secondary-Antibody-Polyclonal/A-11001

Alexa Fluor 488 goat anti-rabbit IgG (A11034) was validated by the vendor. Vendor's website: https://www.fishersci.com/shop/products/anti-rabbit-igg-h-l-alexa-fluor-488-conjugated-polyclonal-thermo-scientific-novex-4/a11034

APC anti-mouse CD8a antibody (100712) was validated by the vendor BioLegend. Vendor's website: https://www.biolegend.com/en-us/products/apc-anti-mouse-cd8a-antibody-150?GroupID=BLG6765

APC anti-mouse CD4 antibody (100412) was validated by the vendor BioLegend. Vendor's website: https://www.biolegend.com/en-us/products/apc-anti-mouse-cd4-antibody-245

Anti-mouse CD8a-FITC antibody (553031, 1:100 dilution) was validated by the vendor BD Bioscience. Vendor's website: https://www.bdbiosciences.com/en-us/products/reagents/flow-cytometry-reagents/research-reagents/single-color-antibodies-ruo/fitc-rat-anti-mouse-cd8a.553031

HRP-conjugated anti-mouse IgA antibody (ab97235, 1:2,000 dilution) was validated by the vendor Abcam. Vendor's website: https://www.abcam.com/goat-mouse-iga-alpha-chain-hrp-ab97235.html?accordion=Documents

HRP-conjugated anti-ferret IgA antibody (618-103-006, 1:2,000 dilution) was validated by the vendor Rockland Immunochemicals. Vendor's website: https://www.rockland.com/categories/secondary-antibodies/ferret-iga-alpha-chain-antibody-618-103-006/

Eukaryotic cell lines

Policy information about cell lines

Cell line source(s)	HEK293T and MDCK.2 cell lines were obtained from ATCC and exhibited cell morphology. HEK293T cells were used for lentiviral production. HEK293T and MDCK.2 cells were used for generation of stable cell lines expressing TEVp protein. Raw264.7 cell line was kindly provided by Dr. Tianhui Hu from Cancer Research Center of Xiamen University and originally obtained from ATCC.
Authentication	All cell lines showed expected cell morphology, and no further authentication was performed.

Mycoplasma contamination	All cell lines were routinely checked for mycoplasma contamination using the MycoAlertTM detection kit (Lonza) and confirmed negative for mycoplasma contamination.
Commonly misidentified lines (See ICLAC register)	None of the cell lines used in this study are listed in the ICLAC database of commonly misidentified cell lines.

Animals and other organisms

Policy information about studies involving animals; ARRIVE guidelines recommended for reporting animal research

Laboratory animals	Housing conditions for animals: 12-hour light/12-hour dark cycle, 24℃ and 50% humidity. Female specific-pathogen-free BALB/c, C57BL/6J, ad BALB/c Nude mice at the age of 6-8 weeks were purchased from GemPharmatech and Vital River Laboratory Animal Technology Co., Ltd. and used to evaluate safety, immunogenicity and protection efficacy of vaccines. Female sero-negative ferrets (Wuxi Cay Ferret Farm, Jiangsu, China) at the age of 4-6 months were used to evaluate safety, immunogenicity and protection efficacy of vaccines. Animal experiments were performed with technical assistances from Shenzhen Institute of Advanced Technology, Chinese Academy of Sciences, Sinovac Biotech Ltd., YuBiolab Ltd., and Peking University, and in accordance with the guidelines of the Institutional Animal Care and Use Committee.
Wild animals	This study did not involve wild animals.
Field-collected samples	This study did not involve samples collected the field.
Ethics oversight	Animal experiments were performed with technical assistances from Shenzhen Institute of Advanced Technology, Chinese Academy of Sciences, Sinovac Biotech Ltd., YuBiolab Ltd., Servicebio Ltd., and Peking University, and in accordance with the guidelines of the Institutional Animal Care and Use Committee.

Note that full information on the approval of the study protocol must also be provided in the manuscript.

Human research participants

Policy information about studies involving human research participants

Population characteristics	The lung tissues were from three patients who participated in an ongoing project of establishing the Human Disease Genetic Resource Bank. Participant #1 (female, 65 years old); Participant #2 (male, 62 years old); Participant #3 (female, 61 years old).
Recruitment	The lung tissues were randomly selected from a library of human lung tissues samples which are collected from patients participating in an ongoing project of establishing the Human Disease Genetic Resource Bank. Informed consent was obtained from all participants in the study.
Ethics oversight	The use of paraffin-embedded and frozen sections of human lung tissue was in accordance with all relevant ethical regulations and approved by the Ethics Committee of West China Hospital of Sichuan University.

Note that full information on the approval of the study protocol must also be provided in the manuscript.

Flow Cytometry

Plots

Confirm that:

☒ The axis labels state the marker and fluorochrome used (e.g. CD4-FITC).

☒ The axis scales are clearly visible. Include numbers along axes only for bottom left plot of group (a 'group' is an analysis of identical markers).

☒ All plots are contour plots with outliers or pseudocolor plots.

☒ A numerical value for number of cells or percentage (with statistics) is provided.

Methodology

Sample preparation	The sample preparation was described in the methods, "Analysis of influenza virus-induced T cell responses by flow cytometry" and "Quantification of M1 antigens presentation".
Instrument	Beckman Coulter CytoFlex S was used for cell sorting.
Software	CytExpert Version 2.4.1 software was used for cell sorting and data analysis.
Cell population abundance	The purity of the post-sorted cells was more than 95% as verified by flow cytometry.

Gating strategy	Events were analyzed by forward and side-scatter followed by live-dead discrimination and indicated protein expression of unstained and stained samples using CytExpert Version 2.4.1 software (Beckman Coulter). The generated histograms demonstrate the positive expression of indicated protein based on the gating strategy against the unstained control.

☒ Tick this box to confirm that a figure exemplifying the gating strategy is provided in the Supplementary Information.